NASA/TM-2011-216875
ARL-TR-5123

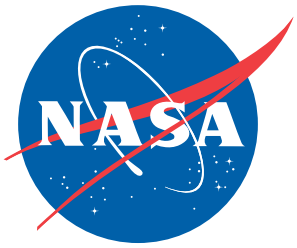

Pre-Test Analysis Predictions for the Shell Buckling Knockdown Factor Checkout Tests – TA01 and TA02

Robert P. Thornburgh
U.S. Army Research Laboratory, Vehicle Technology Directorate
Langley Research Center, Hampton, Virginia

Mark W. Hilburger
Langley Research Center, Hampton, Virginia

January 2011

NASA STI Program . . . in Profile

Since its founding, NASA has been dedicated to the advancement of aeronautics and space science. The NASA scientific and technical information (STI) program plays a key part in helping NASA maintain this important role.

The NASA STI program operates under the auspices of the Agency Chief Information Officer. It collects, organizes, provides for archiving, and disseminates NASA's STI. The NASA STI program provides access to the NASA Aeronautics and Space Database and its public interface, the NASA Technical Report Server, thus providing one of the largest collections of aeronautical and space science STI in the world. Results are published in both non-NASA channels and by NASA in the NASA STI Report Series, which includes the following report types:

- TECHNICAL PUBLICATION. Reports of completed research or a major significant phase of research that present the results of NASA programs and include extensive data or theoretical analysis. Includes compilations of significant scientific and technical data and information deemed to be of continuing reference value. NASA counterpart of peer-reviewed formal professional papers, but having less stringent limitations on manuscript length and extent of graphic presentations.

- TECHNICAL MEMORANDUM. Scientific and technical findings that are preliminary or of specialized interest, e.g., quick release reports, working papers, and bibliographies that contain minimal annotation. Does not contain extensive analysis.

- CONTRACTOR REPORT. Scientific and technical findings by NASA-sponsored contractors and grantees.

- CONFERENCE PUBLICATION. Collected papers from scientific and technical conferences, symposia, seminars, or other meetings sponsored or co-sponsored by NASA.

- SPECIAL PUBLICATION. Scientific, technical, or historical information from NASA programs, projects, and missions, often concerned with subjects having substantial public interest.

- TECHNICAL TRANSLATION. English-language translations of foreign scientific and technical material pertinent to NASA's mission.

Specialized services also include creating custom thesauri, building customized databases, and organizing and publishing research results.

For more information about the NASA STI program, see the following:

- Access the NASA STI program home page at *http://www.sti.nasa.gov*

- E-mail your question via the Internet to help@sti.nasa.gov

- Fax your question to the NASA STI Help Desk at 443-757-5803

- Phone the NASA STI Help Desk at 443-757-5802

- Write to:
  NASA STI Help Desk
  NASA Center for AeroSpace Information
  7115 Standard Drive
  Hanover, MD 21076-1320

NASA/TM-2011-216875
ARL-TR-5123

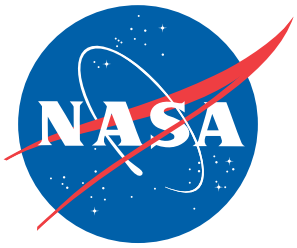

Pre-Test Analysis Predictions for the Shell Buckling Knockdown Factor Checkout Tests – TA01 and TA02

Robert P. Thornburgh
U.S. Army Research Laboratory, Vehicle Technology Directorate
Langley Research Center, Hampton, Virginia

Mark W. Hilburger
Langley Research Center, Hampton, Virginia

National Aeronautics and
Space Administration

Langley Research Center
Hampton, Virginia 23681-2199

January 2011

Available from:

NASA Center for AeroSpace Information
7115 Standard Drive
Hanover, MD 21076-1320
443-757-5802

Preface

The Shell Buckling Knockdown Factor Project (SBKF), NESC Assessment #: 07-010-E, was established in March of 2007 by the NASA Engineering and Safety Center (NESC) in collaboration with the NASA Constellation Program (CxP). The SBKF Project has the goal of developing and experimentally validating improved (i.e., less-conservative, more robust) shell buckling design factors (a.k.a. knockdown factors) and design technologies for launch vehicle structures.

Preliminary design studies indicate that implementation of these new knockdown factors can enable significant weight savings in these vehicles and will help mitigate some of NASA's future launch vehicle development and performance risks, e.g., reduced reliance on large-scale testing, high-fidelity estimates of as-built structural performance, increased payload capability, and improved structural reliability.

To this end, a series of detailed Project Reports are being published to document all results from the SBKF Project and including design trade studies, test article and test facility design, analysis and test data, technology development white papers and state-of-the-art assessments, and finally shell design guidelines to update and/or augment the existing NASA SP series publications for the design of buckling-critical thin-walled shell structures. A select group of significant results, in whole or in part, will be published as NASA Technical Memorandums (TM).

Any documents that are published as a part of this series, that refer to or report specific designs or design, analysis and testing methodologies are to be regarded as guidelines and not as NASA requirements or criteria, except as specified in formal project specifications.

Comments concerning the technical content of this NASA TM are welcomed.

The following Test Reports were combined to create this TM:

SBKF-P2-TR-2008-008; Pre-Test Analysis Report – Test Article 1
SBKF-P2-TR-2009-001; Pre-Test Analysis Report – SBKF-P2-CYL-TA02 Test

Table of Contents

List of Figures

Part 1: Pre-Test Analysis Report – Test Article 1 SBKF-P2-TR-2008-008

Part 2: Pre-Test Analysis Report – SBKF-P2-CYL-TA02 Test

List of Tables

Part 1: Pre-Test Analysis Report – Test Article 1 SBKF-P2-TR-2008-008

Part 2: Pre-Test Analysis Report – SBKF-P2-CYL-TA02 Test

Nomenclature

Acronyms

Al-Li	Aluminum-Lithium
CxP	Constellation Program
kips	Kilopounds (1000 pound force)
lbm	Pounds Mass
lbs	Pounds
LV	Launch Vehicle
LVDT	Linear Variable Differential Transformer
MSFC	Marshall Space Flight Center
NESC	NASA Engineering and Safety Center
SBKF	Shell Buckling Knockdown Factor
TA	Test Article
TM	Technical memorandum

List of Symbols

b_r	Ring Spacing
b_s	Axial stiffener spacing
H	Total panel thickness
h	Stiffener height
L	Cylinder specimen length
M_{cr}	Buckling bending moment
N_{cr}	Running load at buckling
P_{cr}	Total axial load at buckling
P_{limit}	Total axial load at limit point
R	Radius of Cylinder
t	Skin thickness
t_{eff}	Effective orthogrid wall thickness
t_r	Thickness of Rings
t_s	Axial stiffener thickness
Δ_{cr}	Axial end-shortening at buckling
Δ_{limit}	Axial end-shortening at limit point
ε_{cr}	Average axial strain at buckling
ε_{xx}	Axial membrane stain
ε_{yy}	Circumferential membrane strain

Part 1: Pre-Test Analysis Report – Test Article 1

1.0 Introduction

This report summarizes the pre-test analysis predictions for the SBKF-P2-CYL-TA01 shell buckling test that was conducted at the Marshall Space Flight Center (MSFC) in support of the Shell Buckling Knockdown Factor (SBKF) Project, NASA Engineering and Safety Center (NESC) Assessment #: 07-010-E. The test article (TA) is an 8-foot-diameter aluminum-lithium (Al-Li) orthogrid cylindrical shell with similar design features as that of the proposed Ares-I and Ares-V barrel structures. The testing included four sub-critical load sequences, meaning loads that will not cause buckling or failure of the TA, and one test to buckling or failure. The load sequences included uniform axial compression loads and combined axial compression and bending. In support of the testing effort, detailed structural analyses were conducted and the results were used to monitor the behavior of the TA during the testing. A summary of predicted results for each of the five load sequences is presented herein.

2.0 Summary of Results

The first TA design was intended to be a relatively simple and predictable specimen to be used to verify the design methods, experimental setup, loading fixture and testing process in the SBKF test program (see Reference 1 for details on the design). The acreage design chosen for the checkout specimen is shown in Table 2.1. The skin is relatively thick at 0.100 inch to prevent pocket buckling. The stiffeners were chosen to be very short with a small height-to-thickness aspect ratio ($h/t_s = 3$). This resulted in a design with a large radius to effective shell wall thickness ratio (R/t_{eff}) which would be representative of very large launch vehicle (LV) barrel design.

Table 2.1. Acreage design for checkout TA.

Dimensions	Design 1 Checkout
t (in)	0.100
H (in)	0.400
h (in)	0.300
b_s (in)	4.00
t_s (in)	0.100
b_r (in)	4.00
t_r (in)	0.100
R/t_{eff}	230.9
Areal Weight (lbm/in^2)	0.0113

Analysis results are presented using the coordinate system shown in Figure 2.1. Although the TA is 78 inches long, it is clamped on each end by attachment rings that extend 4.625 inches from each end of the TA. The axial coordinate measurements start from the top edge of the lower attachment ring and the circumferential coordinate measurements start from the zero index, which is at the center of Panel A. It is important to note that the circumferential coordinate is positive in the clockwise direction when viewed from the top (or towards the left when the cylinder is viewed from the outside).

Table 2.2 shows the buckling loads from a linear eigen analysis for the checkout TA design subjected to uniform axial compression. The results include both the predicted values for a simple analysis that assumes smeared-stiffener properties in the acreage along with the values for a reinforced design, which includes weld lands and reinforced stiffeners adjacent to the axial weld lands. Also shown are the total load carried by the cylinder (P_{cr}) and the average stress resultant (N_{cr}), along with the end shortening at buckling (Δ_{cr}) and the average axial strain at buckling (Δ_{cr}/L). A bending analysis was also performed on the TA model and a critical bending moment (M_{cr}) of 17.883×10^6 in-lb was calculated. The P_{cr} and M_{cr}

values for the reinforced design are used to determine the applied loading of the TA during subcritical testing (i.e., initial test loading to load levels that do not cause buckling or failure).

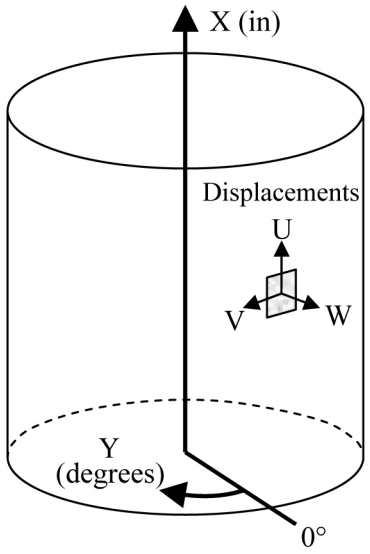

Figure 2.1. Analysis coordinate system.

Table 2.2. Linear buckling response the ideal TA design.

	Smeared	**Reinforced**
P_{cr} (lb)	669,200	714,020
N_{cr} (lb/in)	2219	2368
Δ_{cr} (in)	0.1279	0.1234
ε_{cr} (10–3)	1.850	1.795
Mass (lbm)	235.0	266.9

Detailed measurements of the as-built TA were obtained, giving a mapping of geometric imperfection or deviation from an idealized geometrically perfect cylinder, and were incorporated into the finite-element analysis of the TA. The measured imperfection for the TA installed in the attachment rings is shown in Figure 2.2. Overall, the TA is within 0.1 inch of the nominal geometry. There is some erroneous data across the top edge, due to the presence of the attachment ring, but this was filtered out of the data. Unlike the imperfection used in the design analysis, this imperfection signature shows little influence by the axial weld lands on the overall geometry, and thus indicates the potential for a buckling load very close to the predicted P_{cr} for the perfect cylinder.

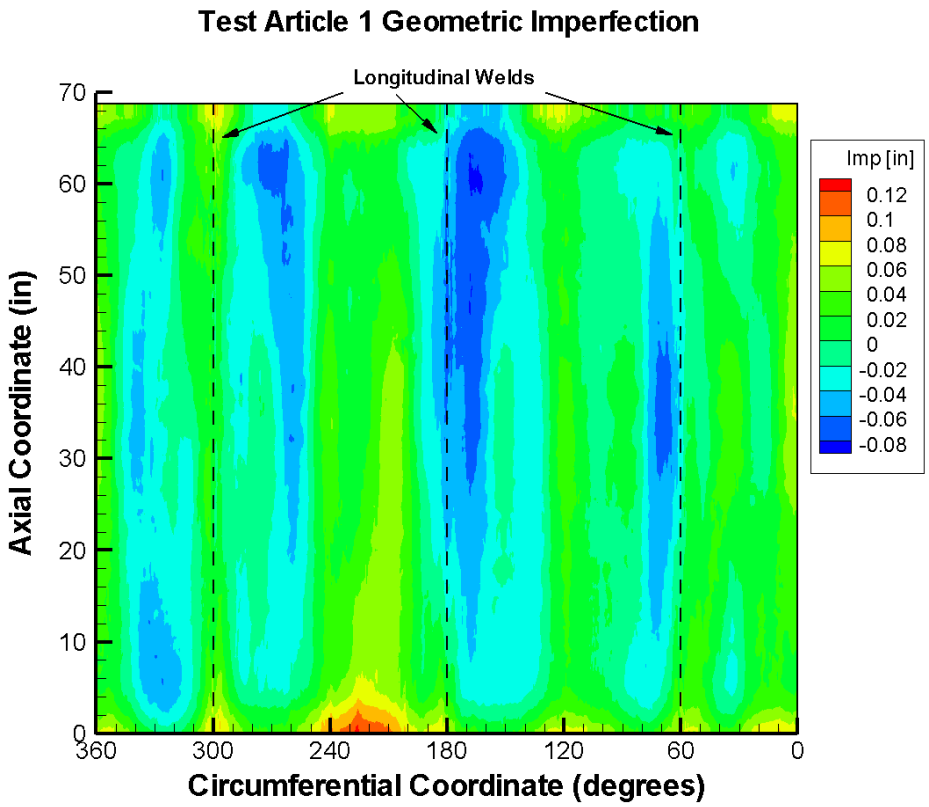

Figure 2.2. Measure geometric imperfection for TA01.

Testing consisted of applying two types of loading to the TA: uniform axial compression and combined bending and axial compression loading in which equal fractions of P_{cr} and M_{cr} are applied simultaneously. A nonlinear static analysis was performed on the imperfect TA for both of these load types up to the buckling limit load. At various load levels a linear eigen analysis was performed to determine the predicted buckling mode shape. By using this method, the nonlinear effect caused by the geometric imperfection can be observed and the mode shape at the limit load can be used to predict the initiation location for the collapse of the cylinder. Finally a nonlinear static analysis combined with a transient collapse analysis was performed to simulate the unstable buckling response of the TA under uniform axial compression. This allows prediction of the post-buckled response of the TA and the remaining load-carrying capability. The finite element model used during the analysis included the load introduction cylinders and the load spiders to predict accurately the effects of the test hardware stiffeners on the response.

The predicted limit load for the cylinder under uniform axial loading was 608,530 lbs, which corresponds to a knockdown factor of 0.852 (85.2% of the classical linear bifuraction buckling load). The load-shortening response of the cylinder with uniform axial compression is shown in Figure 2.3. The prebuckling response of the cylinder is linear and, following collapse, the load is reduced to approximately 235,000 lbs. The increase in end shortening during collapse is a result of strain energy in the test fixtures and loading structure being released. However, the modeling of the test fixtures and loading structure was not exact, so differences in the axial stiffness mean that the end shortening following collapse is not an exact prediction, but is qualitatively correct.

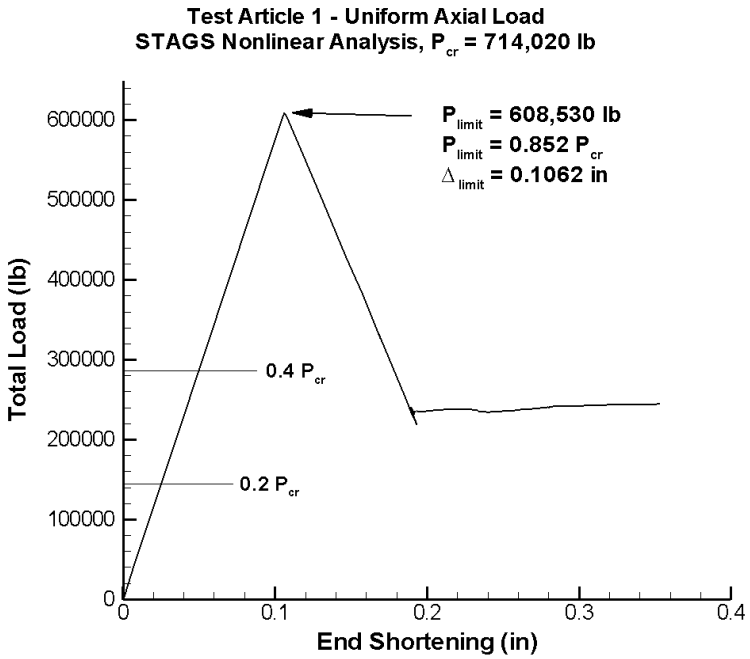

Figure 2.3. Predicted load-shortening response for the TA under uniform axial loading.

The linear bifurcation buckling mode shapes at various load levels are shown in Figure 2.4. The initial unloaded mode shape suggests that buckling will initiate at the axial weld land, but at larger load levels it becomes clear that the nonlinear influence of the imperfection will cause buckling to initiate in the acreage of Panel A. The out-of-plane deformation predicted by a nonlinear analysis at selected load levels is shown in Figure 2.5. An inward deformation can be seen forming near the axial center line of the cylinder. At first glance, the imperfection signature does not suggest this behavior at this region, since there is no distinct inward imperfection present in this location. However, there are two outward imperfection humps on each side of this area, which align with the outward deformation created by the axial compression of the cylinder in the presence of the axial weld lands, as shown in the deformation results at 0.2 P_{cr}. As adjacent areas deform outward, the area where instability initiates is driven inward until the cylinder collapses. Figures 2.6 and 2.7 show the strain at the cylinder outer surface at varying load levels, and the buckling initiation site is the primary area to note. The out-of-plane displacements at the linear variable differential transformer (LVDT) locations are shown in Figures 2.8 and 2.9, and the out-of-plane displacement at the buckling initiation site is shown in Figure 2.10. The LVDTs at the center of Panel A and at the weld lands appear to be the best predictors of the onset of instability.

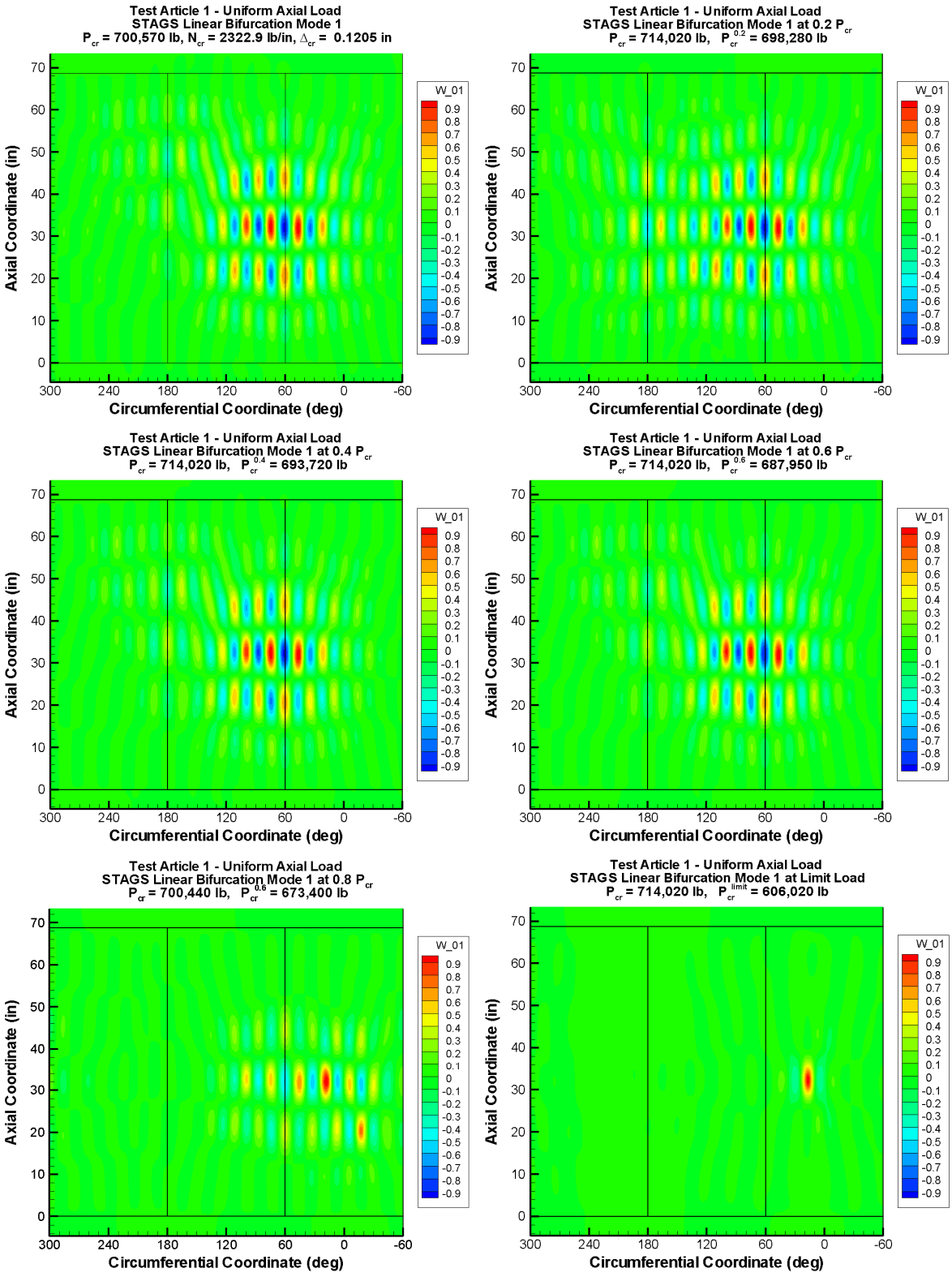

Figure 2.4. Predicted buckling mode shapes at varying load levels for the TA under uniform axial loading.

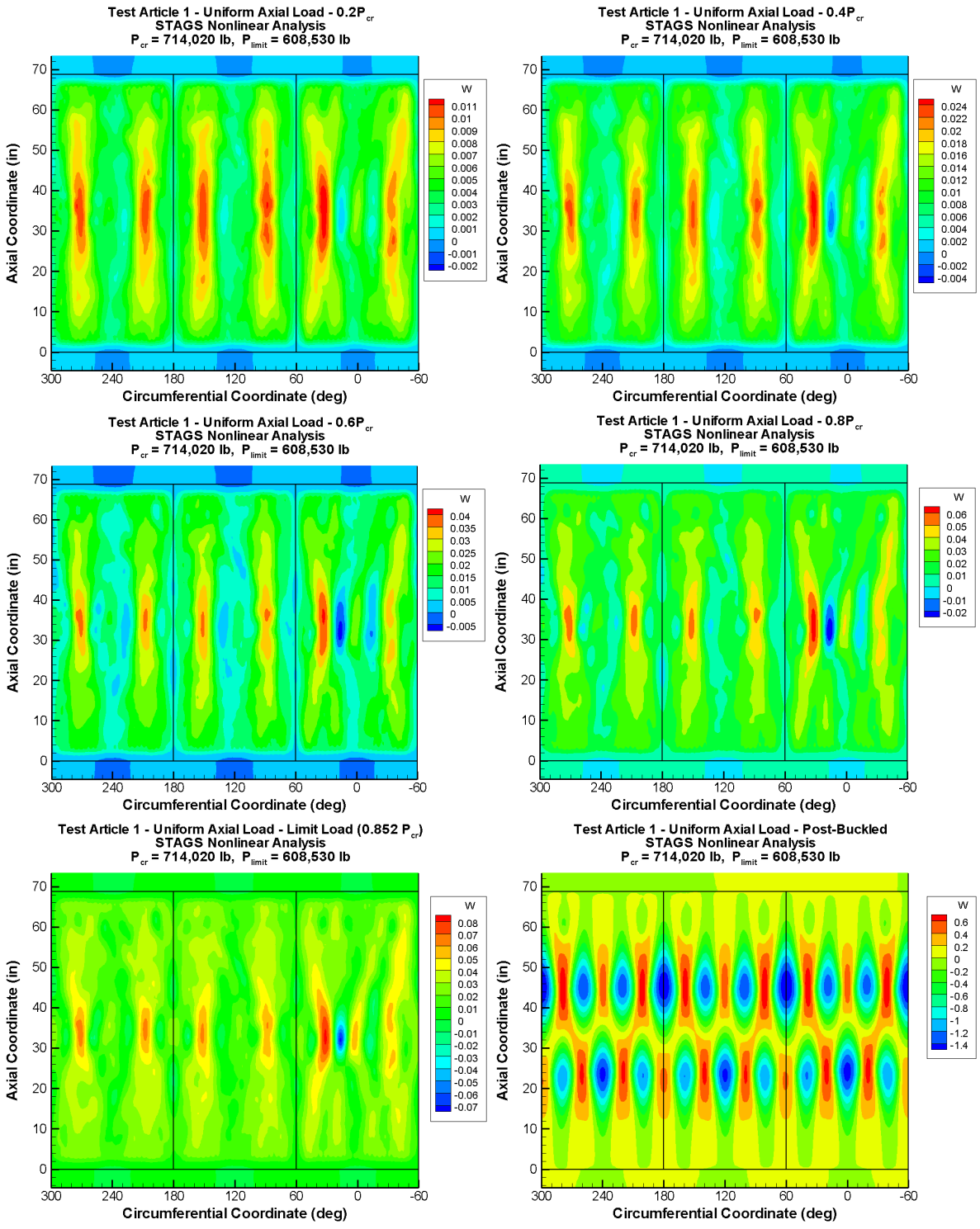

Figure 2.5. Predicted out-of-plane deformation at varying load levels for the TA under uniform axial loading.

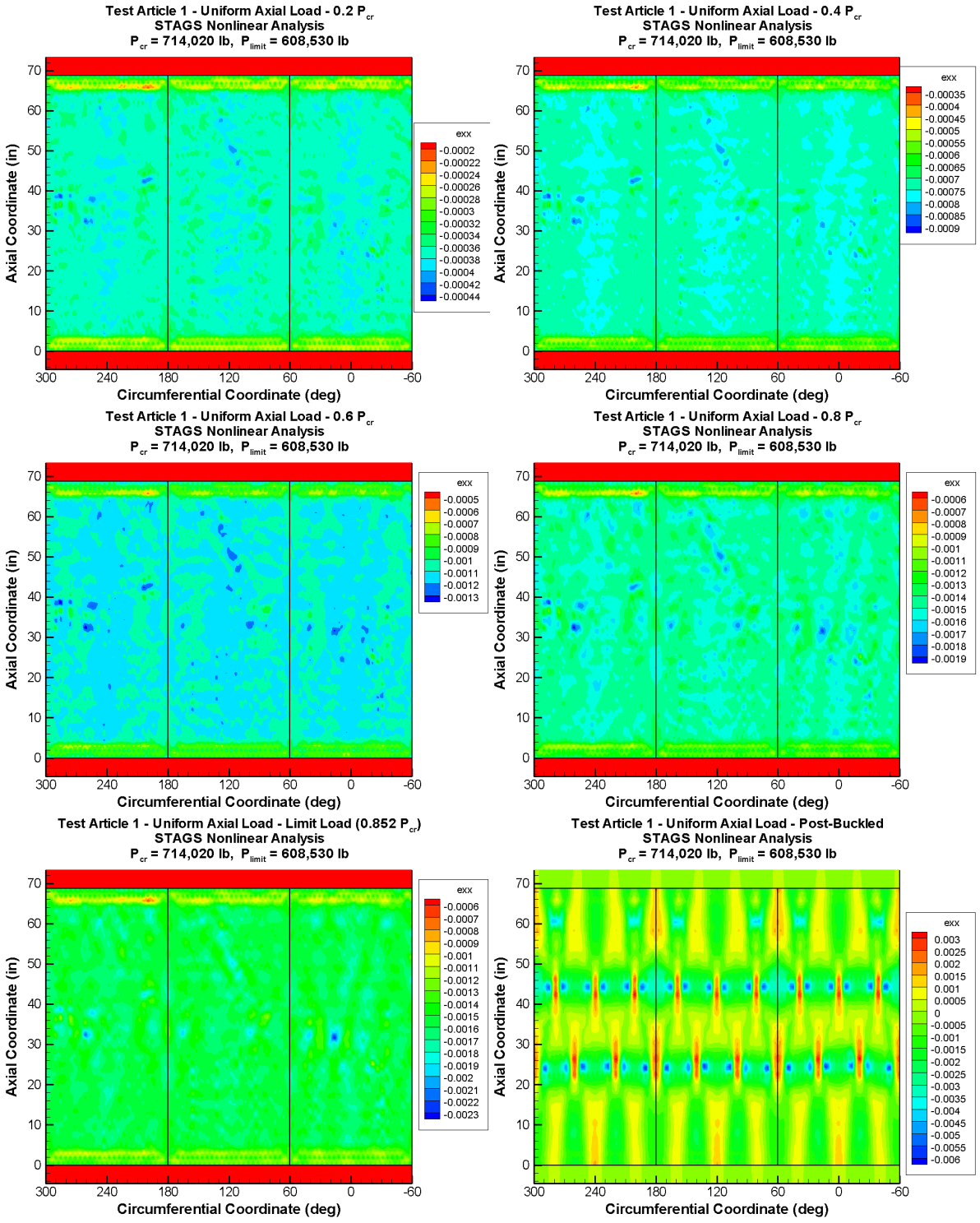

Figure 2.6. Predicted axial strain on the outer surface at varying load levels for the TA under uniform axial loading.

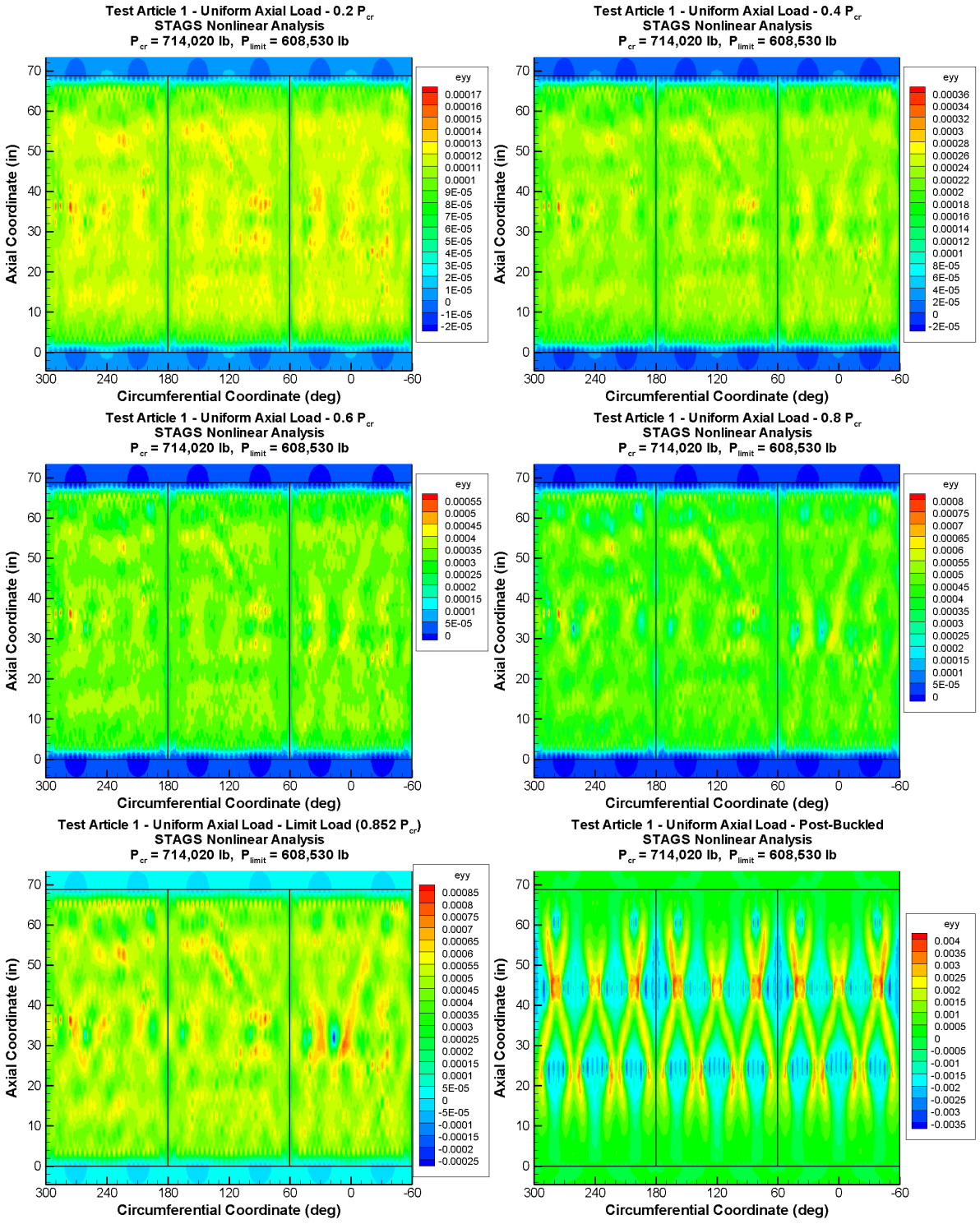

Figure 2.7. Predicted circumferential strain on the outer surface at varying load levels for the TA under uniform axial loading.

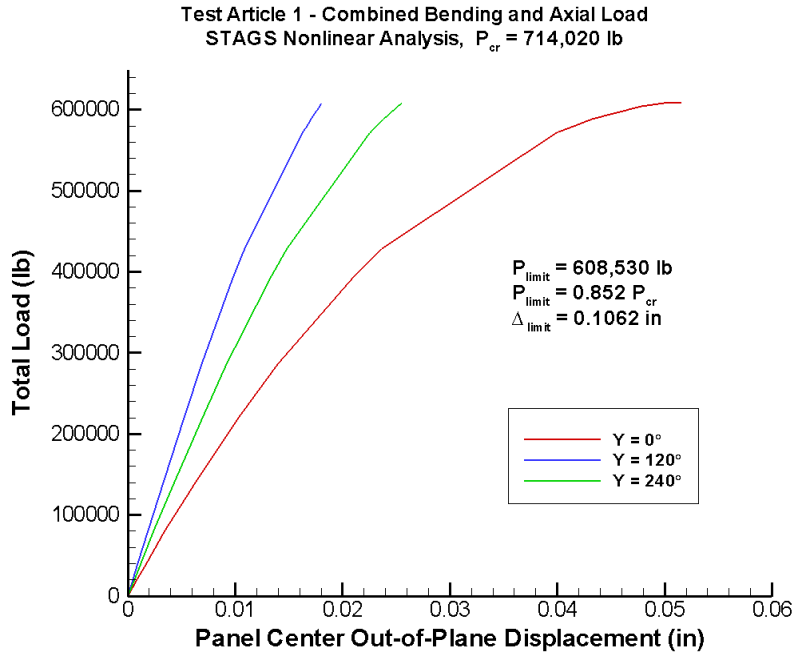

Figure 2.8. Predicted out-of-plane displacement at the center of the panels during uniform axial load.

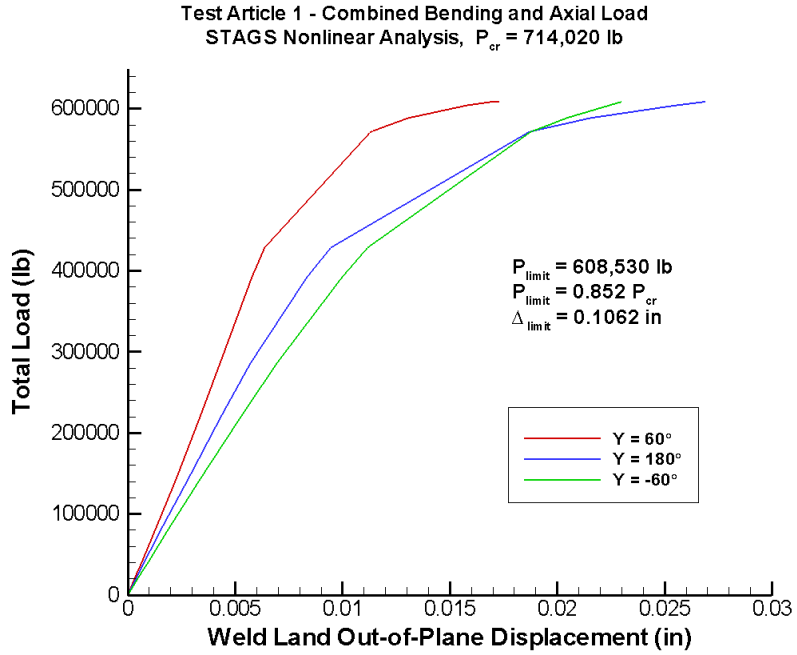

Figure 2.9. Predicted out-of-plane displacement at the center of the axial weld lands during uniform axial load.

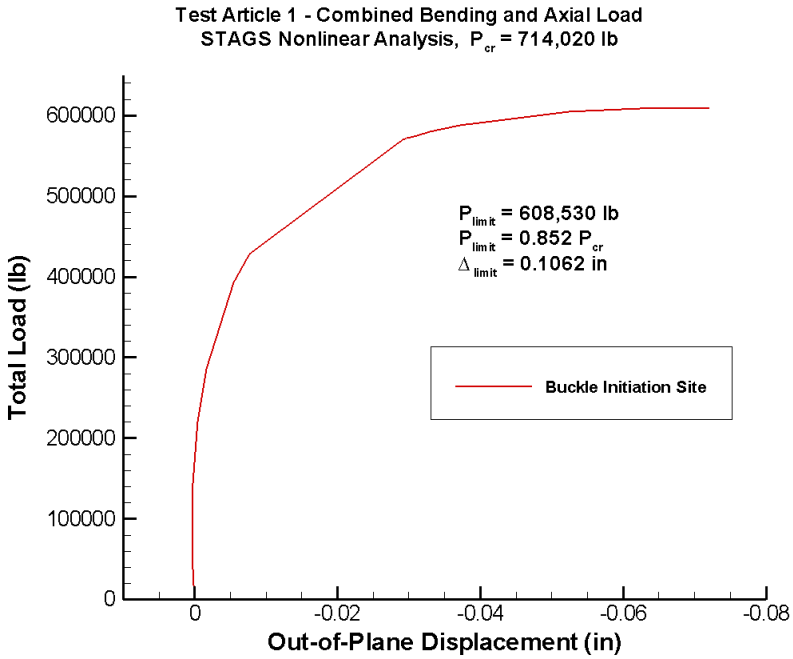

Figure 2.10. Predicted out-of-plane displacement at the dent and buckling initiation site during uniform axial load.

The predicted limit load for the cylinder under combined bending and axial loading was $0.85(0.5P_{cr} + 0.5M_{cr})$. The load-shortening response of the cylinder with combined bending and axial loading at the LVDT locations used during testing is shown in Figure 2.11. LVDT 1 is at 0° where peak compression occurs. LVDTs 2, 3 and 4 are at 90°, 180°, and 270°, respectively. The prebuckling response of the cylinder is linear.

The predicted buckling mode shape from an eigen analysis at the limit load (Figure 2.12) shows that buckling under combined bending and axial load initiates at the same location as the uniform axial load case. The out-of-plane deformation predicted from a nonlinear analysis for selected load levels is shown in Figure 2.13. The deformation response of the cylinder is dominated by global bending as expected. Figures 2.14 and 2.15 show the strain at the cylinder outer surface at varying load levels. The buckling initiation site is the primary area of note. The out-of-plane displacement at the LVDT locations are shown in Figures 2.16 and 2.17, and the out-of-plane displacement at the dent and the buckling initiation site are shown in Figure 2.18. For this load case only the LVDT at the center of Panel A is a good predictor for the onset of instability.

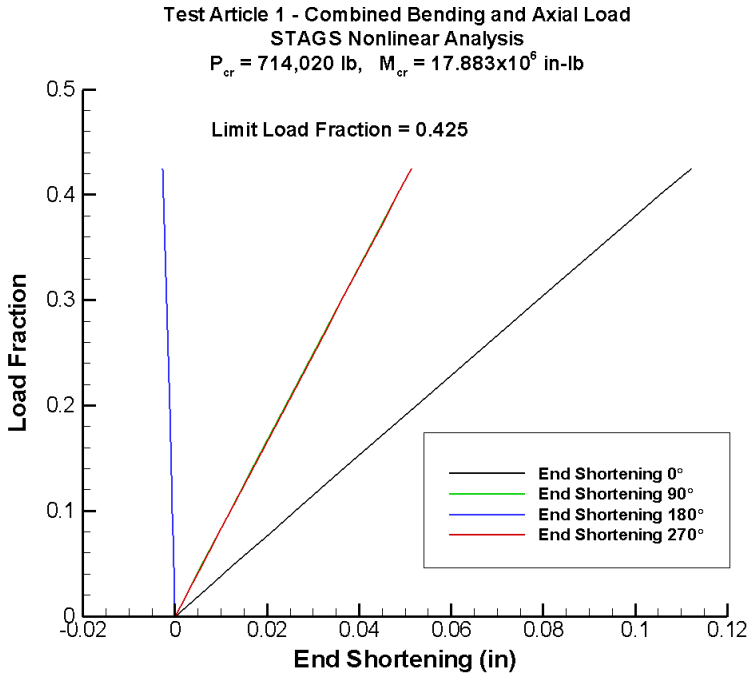

Figure 2.11. Predicted load-shortening response for the TA under combined bending and axial loading.

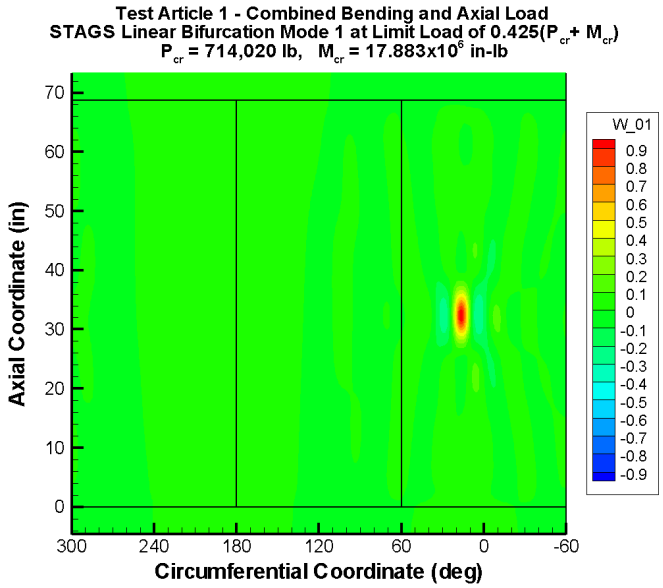

Figure 2.12. Predicted buckling mode shape for the TA under combined bending and axial loading based on eigen analysis at the limit load.

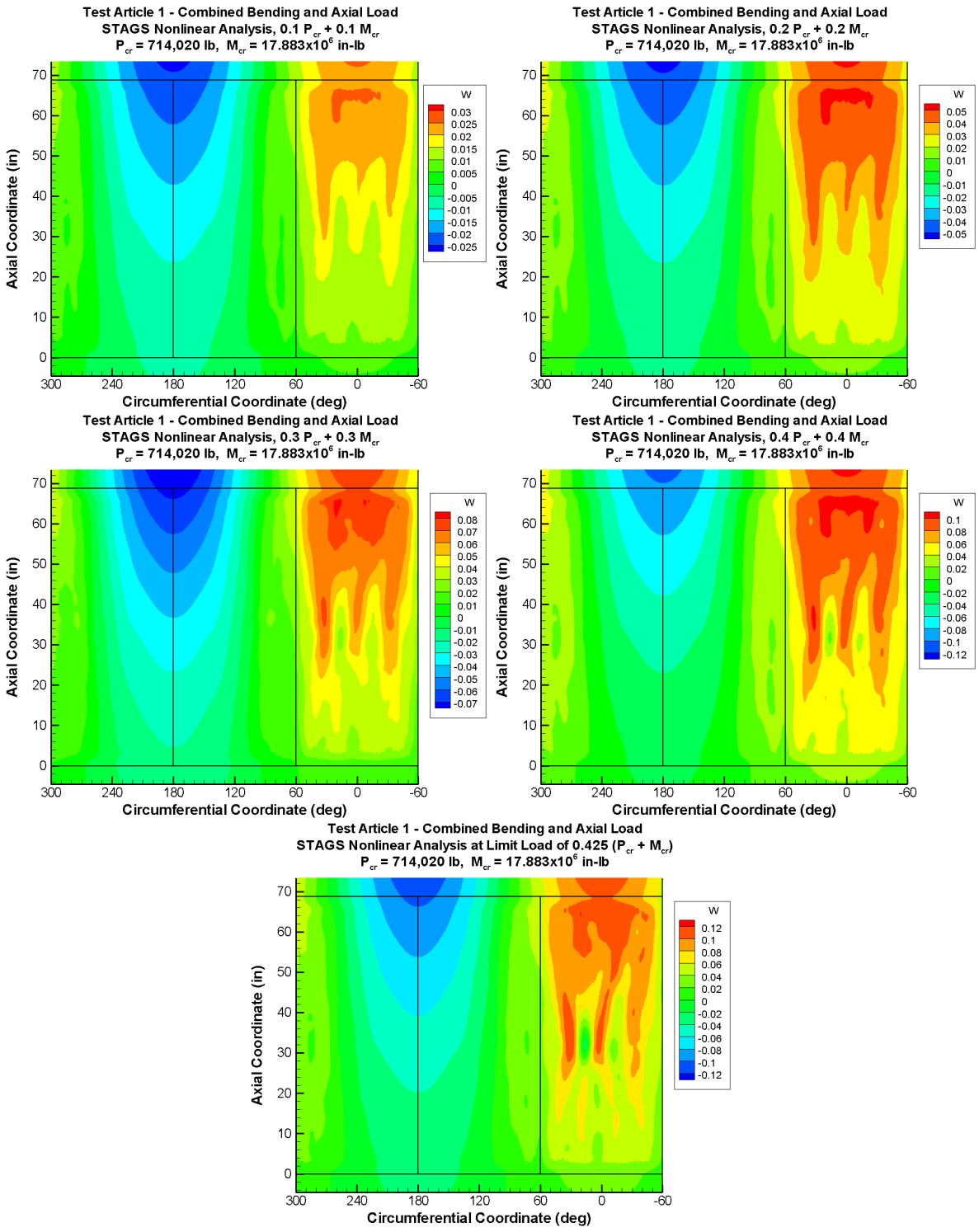

Figure 2.13. Predicted out-of-plane deformation at varying load levels for the TA under combined bending and axial loading.

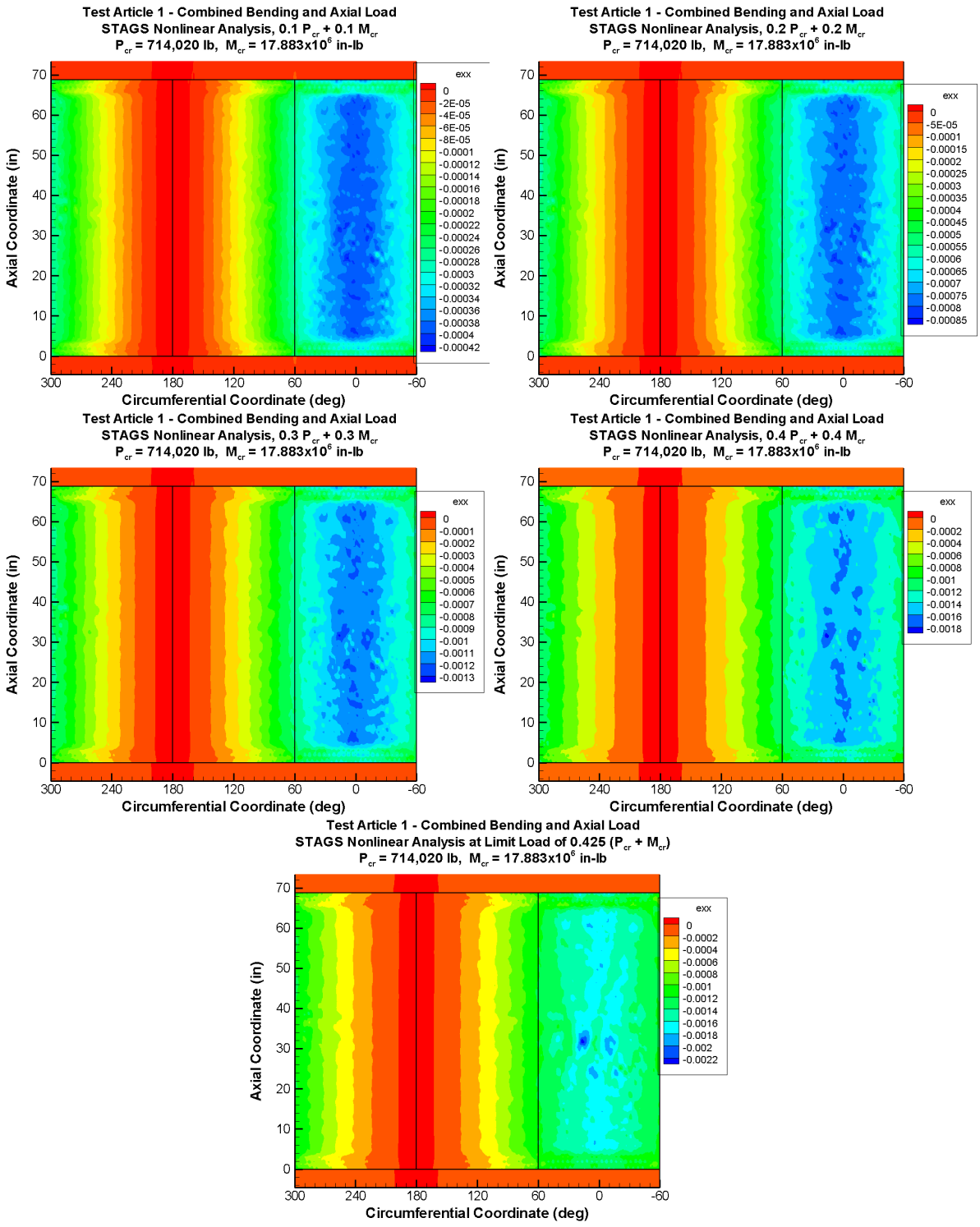

Figure 2.14. Predicted axial strain at varying load levels for the TA under combined bending and axial loading.

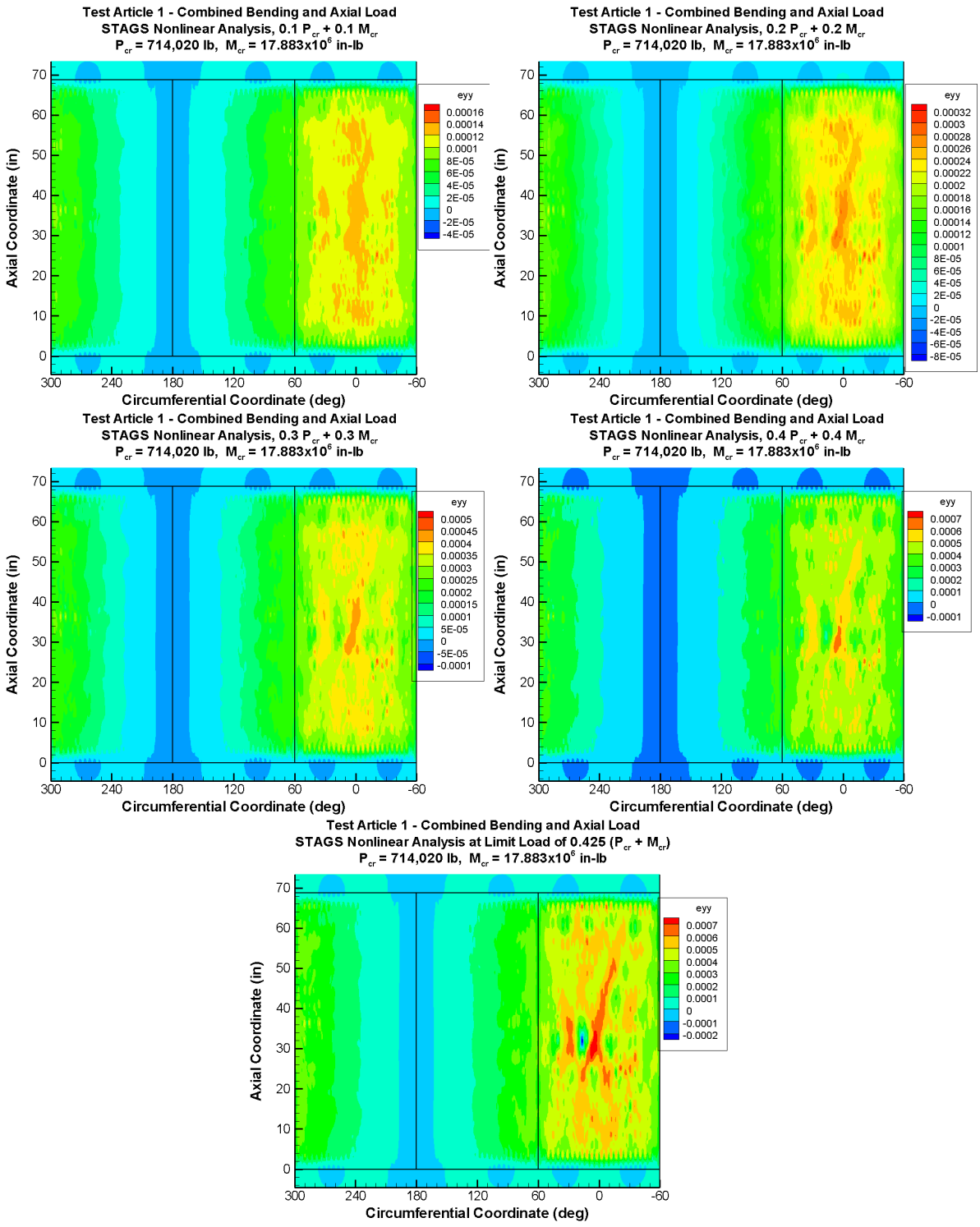

Figure 2.15. Predicted circumferential strain at varying load levels for the TA under combined bending and axial loading.

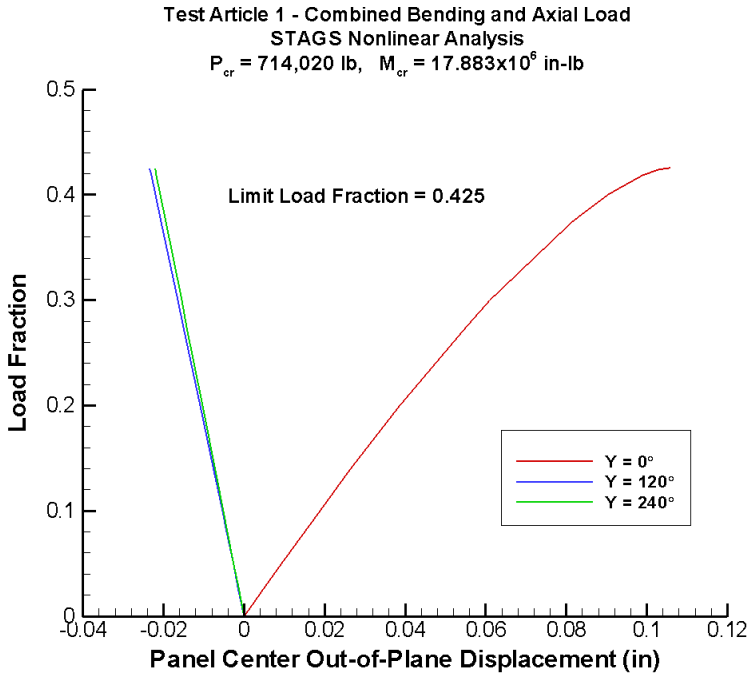

Figure 2.16. Predicted out-of-plane displacement at the center of the panels during combined bending and axial load.

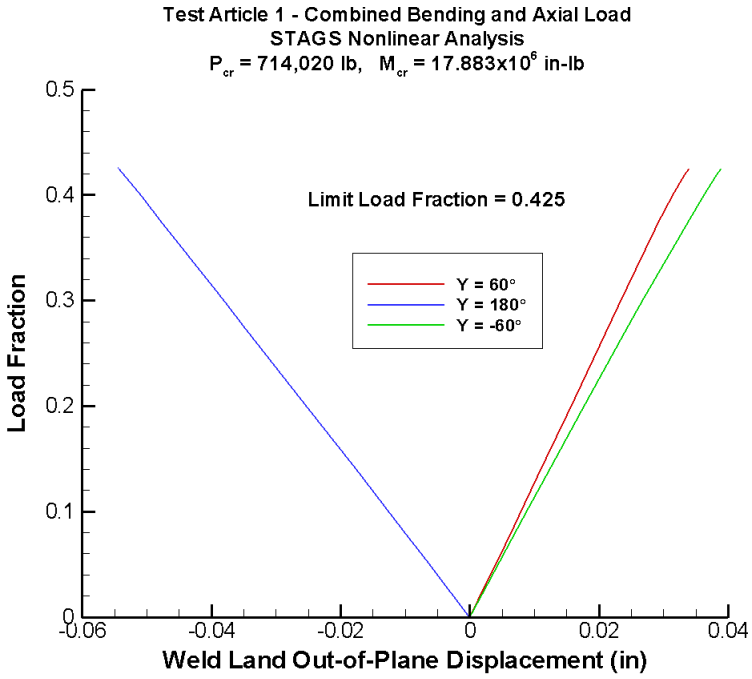

Figure 2.17. Predicted out-of-plane displacement at the center of the axial weld lands during combined bending and axial load.

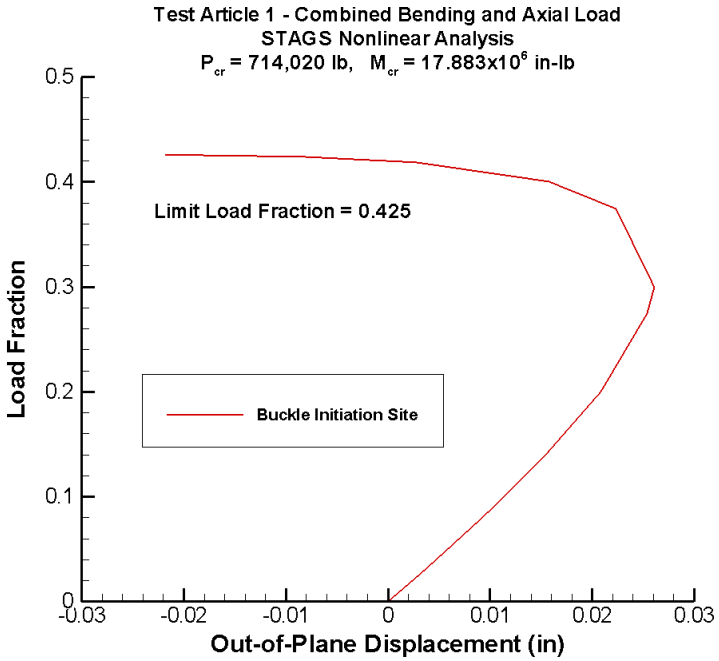

Figure 2.18. Predicted out-of-plane displacement at the dent and buckling initiation site during combined bending and axial load.

3.0 References

1. Thornburgh, R. P.; and Hilburger, M. W.: *Design of Orthogrid Cylinder Test Articles for the Shell Buckling Knockdown Factor Assessment*. NASA/TM-2010-216866, November 2010.

Part 2: Pre-Test Analysis Report – SBKF-P2-CYL-TA02 Test

1.0 Introduction

This report summarizes the pre-test analysis predictions for the SBKF-P2-CYL-TA02 shell buckling test that was conducted at the MSFC in support of the SBKF Project, NESC Assessment #: 07-010-E. The TA is an 8-foot-diameter Al-Li orthogrid cylindrical shell with similar design features as that of the proposed Ares-I and Ares-V barrel structures. The testing included three sub-critical load sequences, meaning loads that will not cause buckling or failure of the TA and two tests to buckling or failure. The load sequences included uniform axial compression loads and combined axial compression and bending. In support of the testing effort, detailed structural analyses were conducted and the results used to monitor the behavior of the TA during the testing. A summary of these results is presented herein.

2.0 Summary of Results

The second TA, TA02, used the same stiffener design as the first TA, TA01, but was intended to be tested to failure with combined bending and axial loading. The TA design was intended to be a relatively simple and predictable specimen used to verify the design methods, experimental setup, loading fixture and testing process in the SBKF test program. See Reference 1 for more information on the TA02 design. The acreage design chosen for the checkout specimen is shown in Table 2.1. The skin was relatively thick at 0.100 inch to prevent pocket buckling. The stiffeners were chosen to be very short with a small height-to-thickness aspect ratio ($h/t_s = 3$). This results in design with a large radius to effective shell wall thickness ratio (R/t_{eff}) which would be representative of a very large launch vehicle barrel design.

Table 2.1. Acreage design for checkout TA.

Dimensions	Design 1 Checkout
t (inch)	0.100
H (inch)	0.400
h (inch)	0.300
b_s (inch)	4.00
t_s (inch)	0.100
b_r (inch)	4.00
t_r (inch)	0.100
R/t_{eff}	230.9
Areal Weight (lbm/in^2)	0.0113

Analysis results are presented using the coordinate system shown in Figure 2.1. The TA is 78 inches long and was clamped on each end by attachment rings that extended 4.625 inches from each end of the TA. The axial coordinate measurements start from the top edge of the lower attachment ring and the circumferential coordinate measurements start from the zero index, which is at the center of Panel A. It is important to note that the circumferential coordinate was positive in the clockwise direction when viewed from the top (or towards the left when the cylinder is viewed from the outside). For this test, bending moment was applied about the axis formed by Y = 270º, and positive bending moment was defined such that maximum axial compression of the TA occurs at Y = 0º.

The buckling loads predicted from a linear eigen analysis of the checkout TA design subjected to uniform axial compression are shown in Table 2.2. The results include both the predicted values for a simple, smeared-stiffener analysis of the acreage along with the values for a reinforced design, which includes weld lands and reinforced stiffeners adjacent to the axial weld lands. The total load carried by the cylinder (P_{cr}) and the average stress resultant (N_{cr}) are shown, along with the end shortening at buckling (Δ_{cr}) and the average axial strain at buckling (Δ_{cr}/L). A bending analysis was also performed on the TA design and

a critical bending moment (M_{cr}) of 17.883 × 10^6 in-lb was calculated. The P_{cr} and M_{cr} values for the reinforced design were used to determine the applied loading of the TA during subcritical testing.

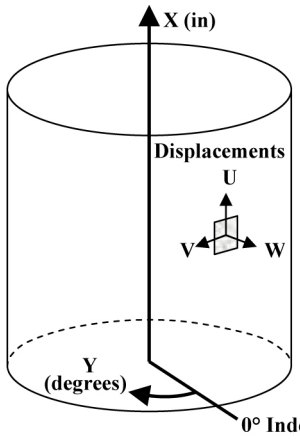

X = 0 Corresponds to top edge of lower attachment ring.
All displacements are relative to local shell surface.

Figure 2.1. Analysis coordinate system.

Table 2.2. Linear buckling response the ideal TA design.

	Smeared	**Reinforced**
P_{cr} (lb)	669,200	714,020
N_{cr} (lb/in)	2219	2368
Δ_{cr} (inch)	0.1279	0.1234
ε_{cr} (10^{-3})	1.850	1.795
Mass (lbm)	235.0	266.9

Detailed measurements of the as-built TA were obtained, giving a mapping of geometric imperfection or deviation from an idealized geometrically perfect cylinder, and were incorporated into the finite-element analysis of the TA. The measured imperfection for the TA installed in the attachment rings is shown in Figure 2.2. Overall, the TA is within 0.1 inch of the nominal geometry and is very similar to the measured geometry of TA01. There was some erroneous data across the top edge, due to the presence of the attachment ring, but this was filtered out of the data. Unlike the imperfection used in the design analysis, this imperfection signature shows little influence by the axial weld lands on the overall geometry, and thus indicates the potential for a buckling load very close to the predicted P_{cr} for the perfect cylinder.

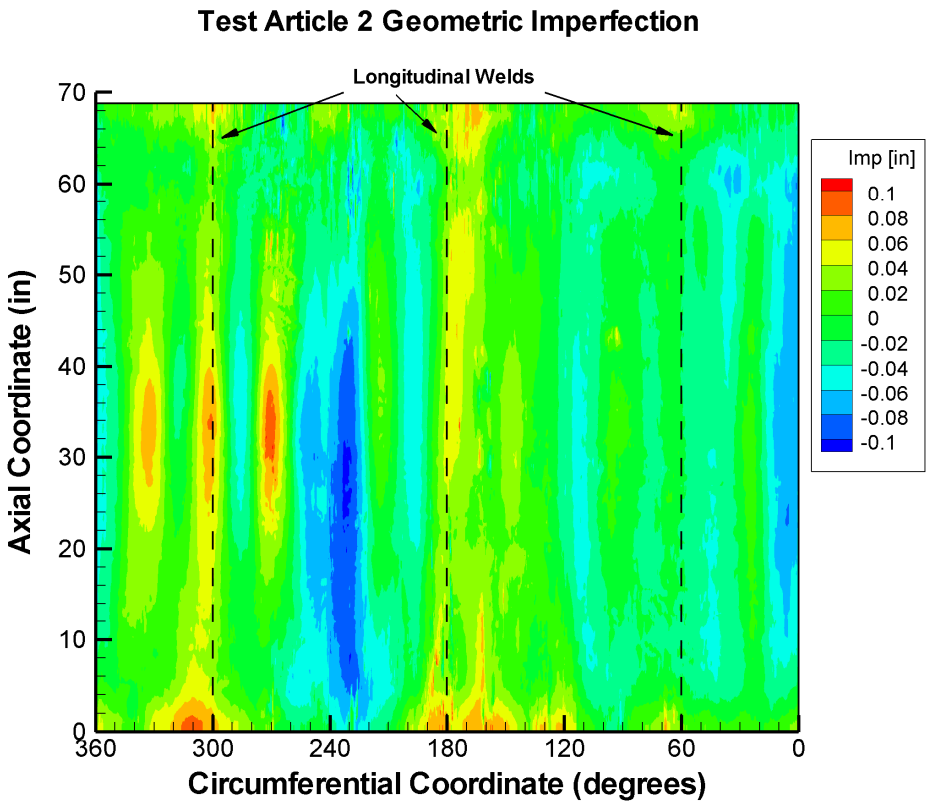

Figure 2.2. Measure geometric imperfection for TA02.

Testing consisted of applying three types of loading to the TA: uniform axial compression and two combined bending and axial load cases. For the combine load cases, bending and compression are applied in a ratio of 3:2, respectively, with one case using a positive bending moment and the other using a negative bending moment. This allows the TA to be tested to failure twice, once with the maximum compression occurring at the center of Panel A (0º) and once with the maximum compression occurring at the weld land between panels B and C (180º). A nonlinear static analysis was performed on the imperfect TA for each of these load cases up to the buckling limit load. At various load levels during the nonlinear analysis, a linear eigen analysis was performed to determine the predicted buckling mode shape. By using this method, the nonlinear effect caused by the geometric imperfection can be observed and the mode shape at the limit load can be used to predict the initiation location for the collapse of the cylinder. Finally, a nonlinear static analysis combined with a transient collapse analysis was performed to simulate the unstable collapse of the TA under combined bending and axial compression. This allows prediction of the post-buckled response of the TA and the remaining load carrying capability. The finite-element model used during the analysis included the load introduction cylinders and the load spiders. The modeling approach used for this loading structure has been improved, since the pre-test predictions were performed for the first TA, TA01, and the model used herein more closely replicates the physics of the load system used during the test.

The predicted limit load for the cylinder under uniform axial loading was 554,370 lbs, which corresponds to a knockdown factor of 0.776. The load-shortening response of the cylinder with uniform axial compression is shown in Figure 2.3, and the pre-buckling response of the cylinder is very linear.

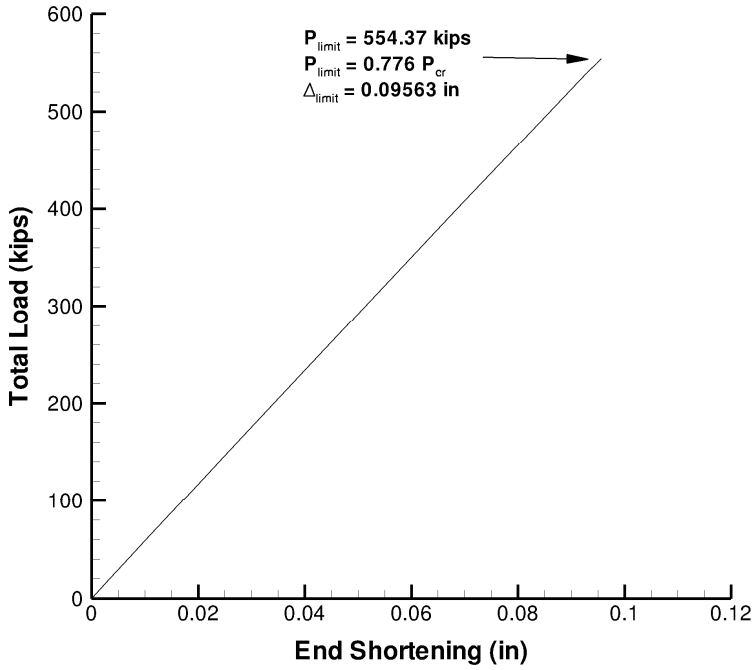

Figure 2.3. Predicted load-shortening response for the TA under uniform axial loading.

The out-of-plane deformation at 0.2 P_{cr} is shown in Figure 2.4 along with the strain at the cylinder outer surface. The out-of-plane deformation and outer surface strains at the limit load of 554.37 kips are shown in Figure 2.5. An inward deformation can be seen forming near the mid-length of the cylinder at 160º. This location is the predicted buckling initiation site for this TA under uniform axial load. The out-of-plane displacement at the linear variable differential transformer (LVDT) locations to be used during the test are shown in Figures 2.6 and 2.7. The LVDTs all show a significant amount of nonlinearity and should be good indicators of the onset of instability.

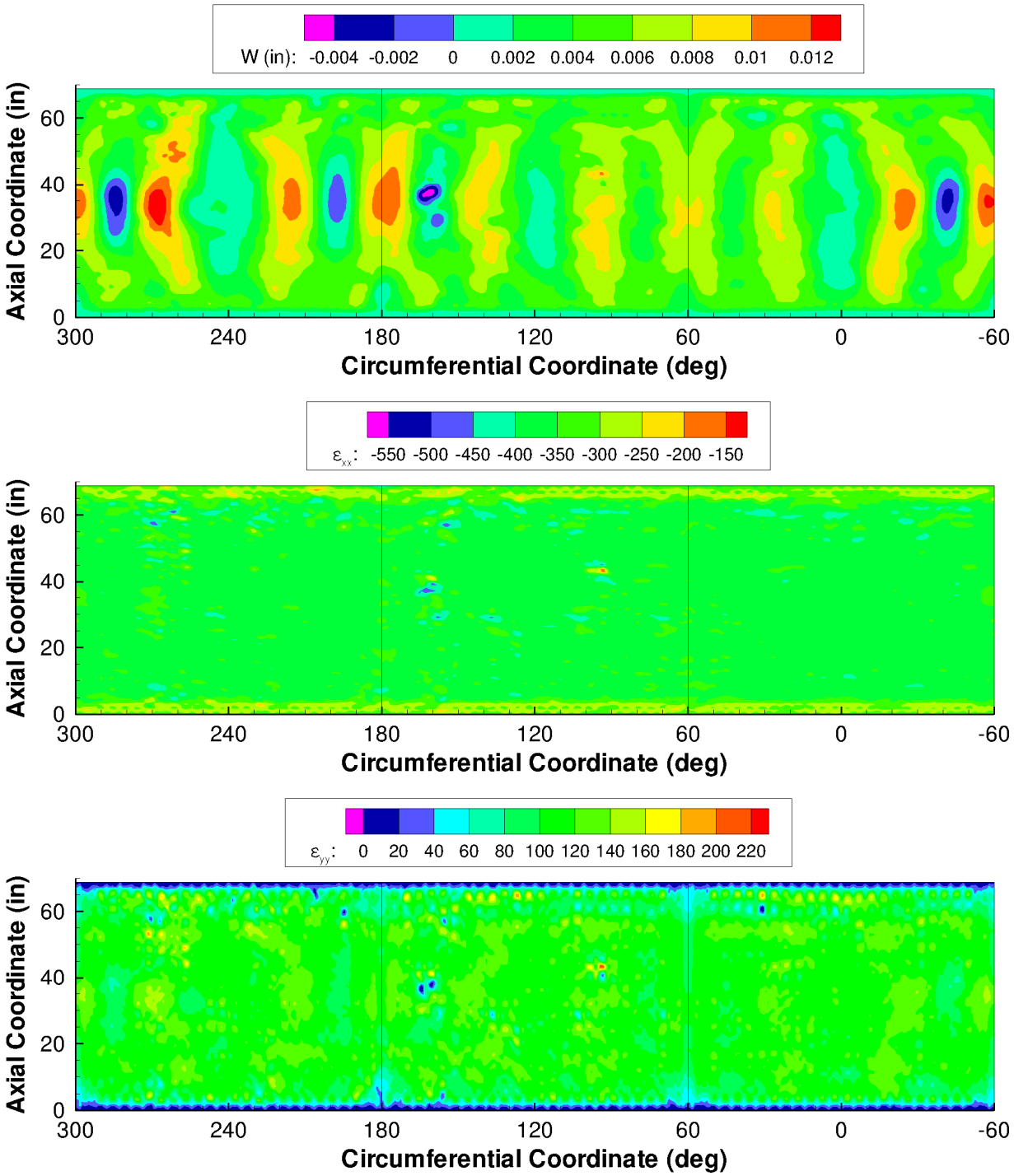

Figure 2.4. Predicted out-of-plane deformation and outer surface strains for the TA under uniform axial loading at 0.20 P_{cr}.

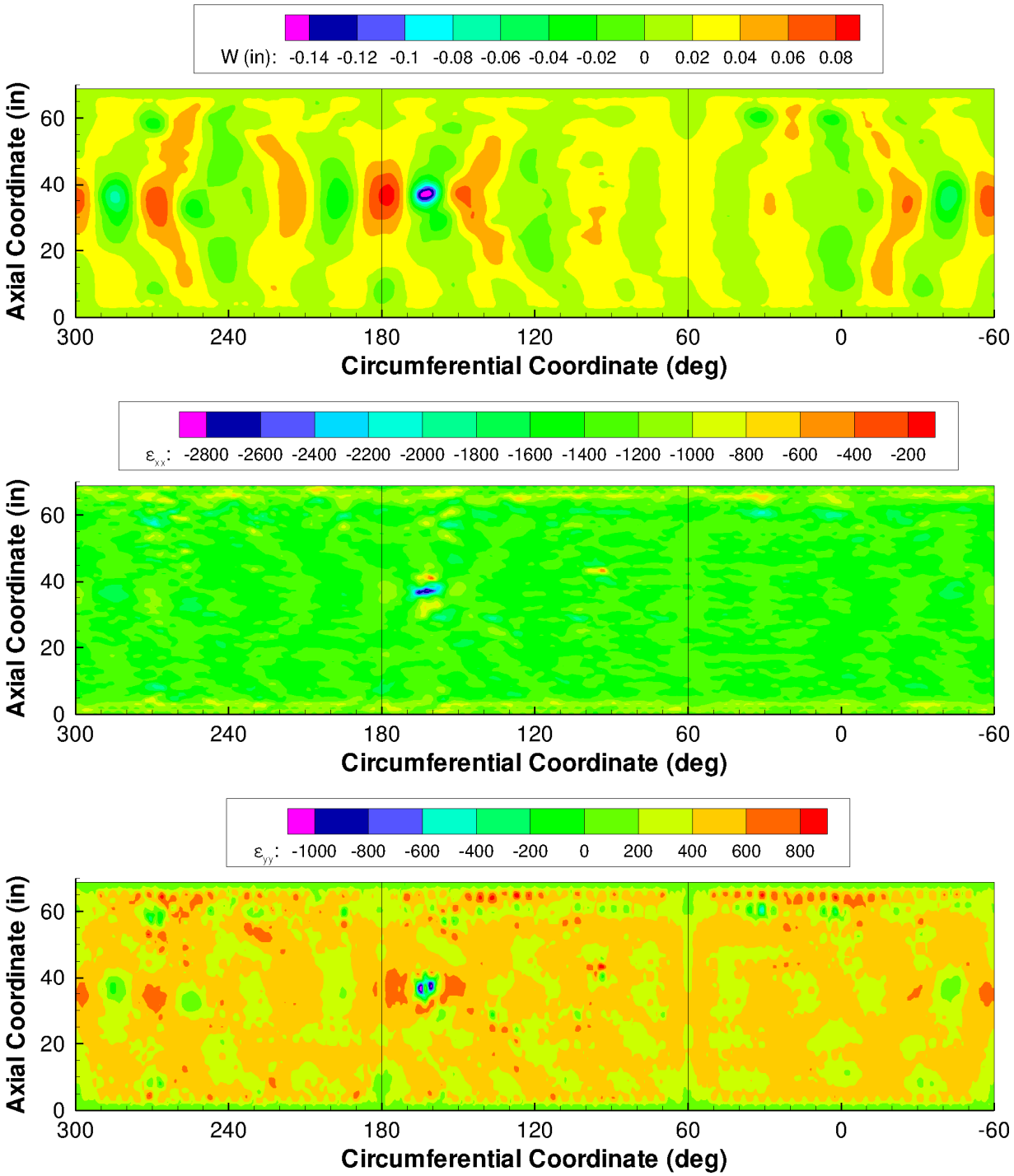

Figure 2.5. Predicted out-of-plane deformation and outer surface strains for the TA under uniform axial loading at limit load of 554.37 kips.

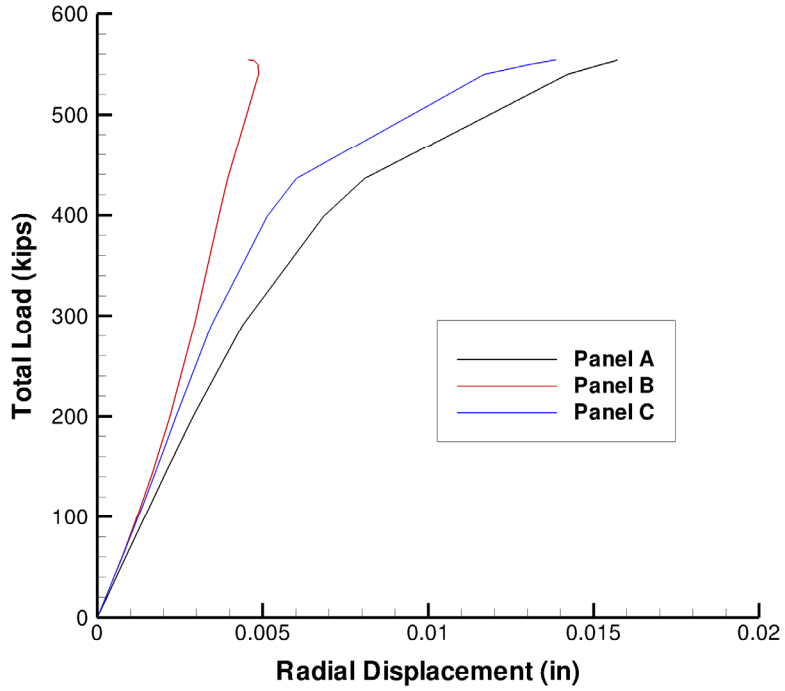

Figure 2.6. Predicted out-of-plane displacement at the center of the panels during uniform axial load.

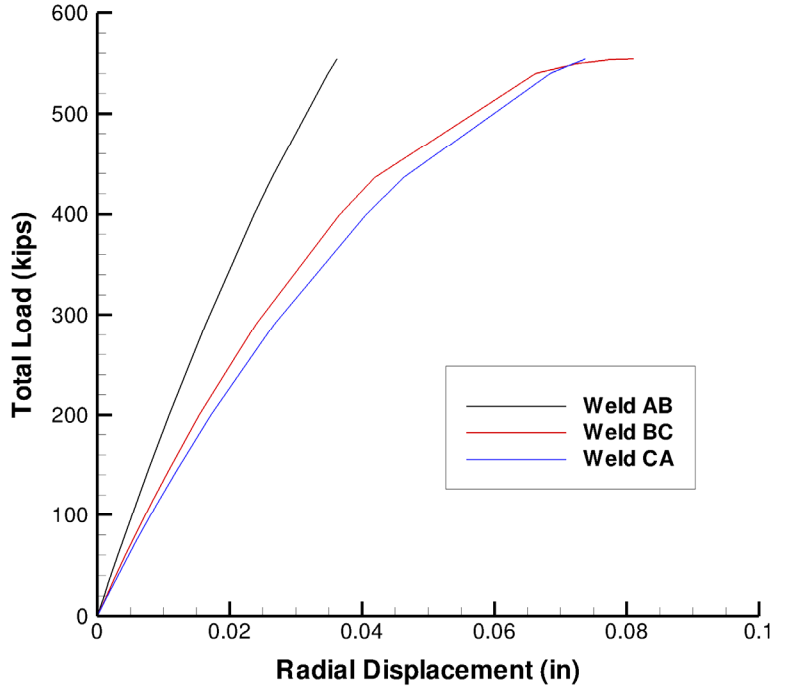

Figure 2.7. Predicted out-of-plane displacement at the center of the axial weld lands during uniform axial load.

For the combined bending and axial loading cases, an eigen analysis and a nonlinear analysis were first performed on the TA without any geometric imperfection included in the model. For the load case with a positive bending moment (maximum compression in Panel A), the predicted linear buckling load $1.050(0.4P_{cr} + 0.6M_{cr})$, and the resulting mode shape is shown in Figure 2.8. The nonlinear limit load for this case was $1.044(0.4P_{cr} + 0.6M_{cr})$ and the buckling initiated with the same deformation pattern shown by the linear eigen mode shape.

Next, the measured geometric imperfection was included in the model and nonlinear analysis was used to predict the expected limit loads, and a transient collapse analysis was performed to simulate the failure. The nonlinear limit load for the case with positive bending moment and maximum compression in Panel A was $0.8305(0.4P_{cr} + 0.6M_{cr})$, and the resulting end-shortening response curve is shown in Figure 2.9. The pre-buckling response is linear and following buckling the TA is still carrying seventy percent of the pre-buckling load. Out-of-plane deformation and outer surface strains are shown for $(0.2P_{cr} + 0.3M_{cr})$, $(0.3P_{cr} + 0.45M_{cr})$, limit load and post-buckled in Figures. 2.10-2.13, respectively. These results show an inward deformation forming ten inches from the top of the TA at 0º, and it is at this location that buckling is predicted to initiate for this load case. The large post-buckled deformation is largely confined to Panel A, and the strains are significantly less than the yield strain for Al-Li. Thus, the second load sequence to failure should not be significantly influenced by this load case. The radial displacements at the center of the panels and the center of the axial weld lands are shown in Figures 2.14 and 2.15. Of these, the LVDT at the center of Panel A appears to be the best predictor of the onset of instability.

The analysis of the TA without any geometric imperfection and with negative bending moment (maximum compression along the BC weld land), predicted a linear buckling load $1.062(0.4P_{cr} + 0.6M_{cr})$, and the resulting mode shape is shown in Figure 2.16. The nonlinear limit load for this case was $1.027(0.4P_{cr} + 0.6M_{cr})$.

Next, the measured geometric imperfection was included in the model and nonlinear analysis was used to predict the expected test limit loads, and a transient collapse analysis was performed to simulate the failure. The nonlinear limit load for the case with positive bending moment and maximum compression in Panel A was $0.7919(0.4P_{cr} + 0.6M_{cr})$, and the resulting end shortening prediction is shown in Figure 2.17. The pre-buckling response is linear and following buckling the TA is still carrying seventy percent of the pre-buckling load. Out-of-plane deformation and outer surface strains are shown for $(0.2P_{cr} + 0.3M_{cr})$, $(0.3P_{cr} + 0.45M_{cr})$, limit load and post-buckled in Figures 2.18-2.21, respectively. These results show an inward deformation forming at the center of the TA near 165º adjacent to the weld land, and it is at this location that buckling is predicted to initiate for this load case. The radial displacements at the center of the panels and the center of the axial weld lands are shown in Figures 2.22 and 2.23. Of these, the LVDT at the center of Panel A was the best indicator of the onset of instability.

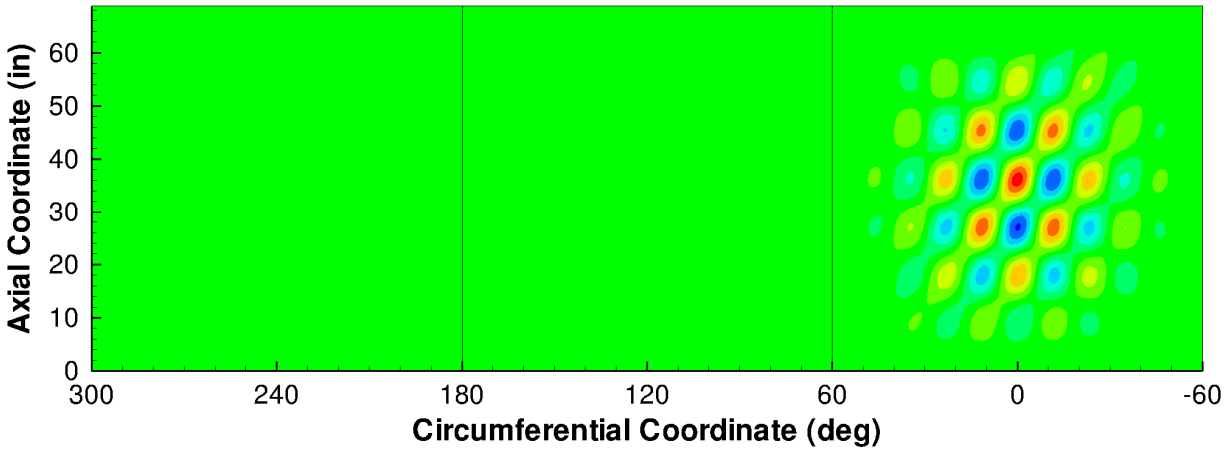

Figure 2.8. Predicted buckling mode shape for the TA under combined axial loading and positive bending.

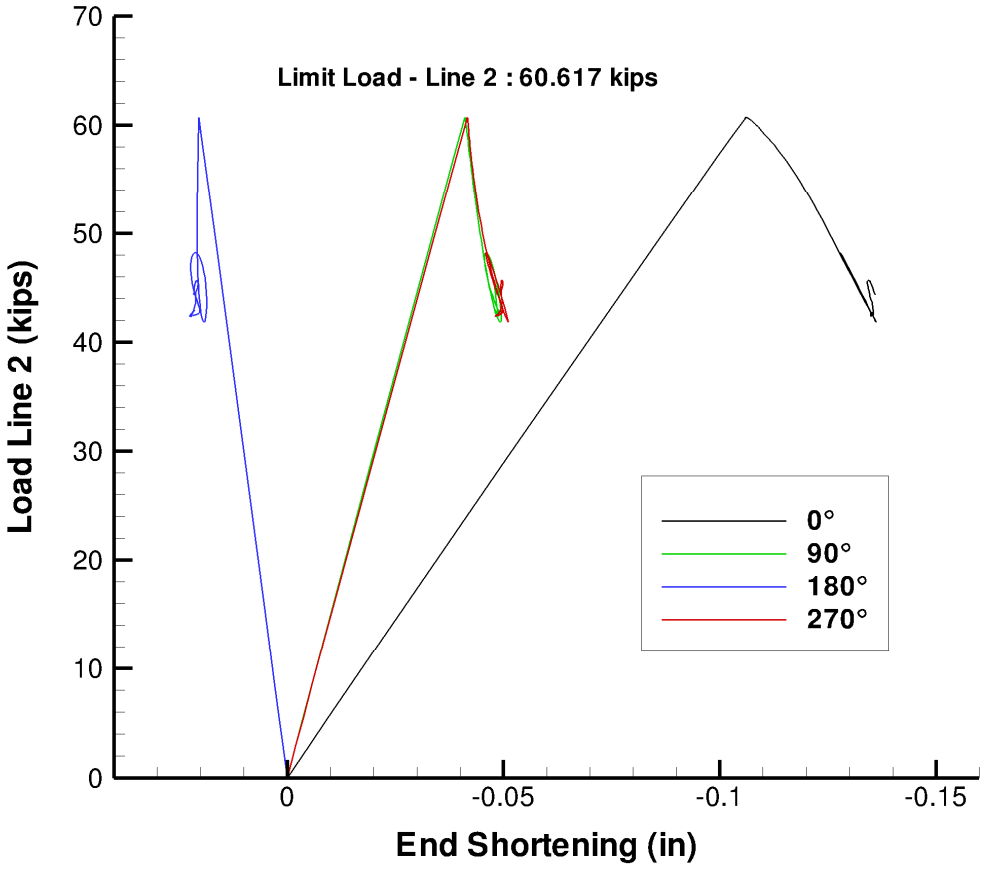

Figure 2.9. Predicted load-shortening response for the TA under combined axial loading and positive bending.

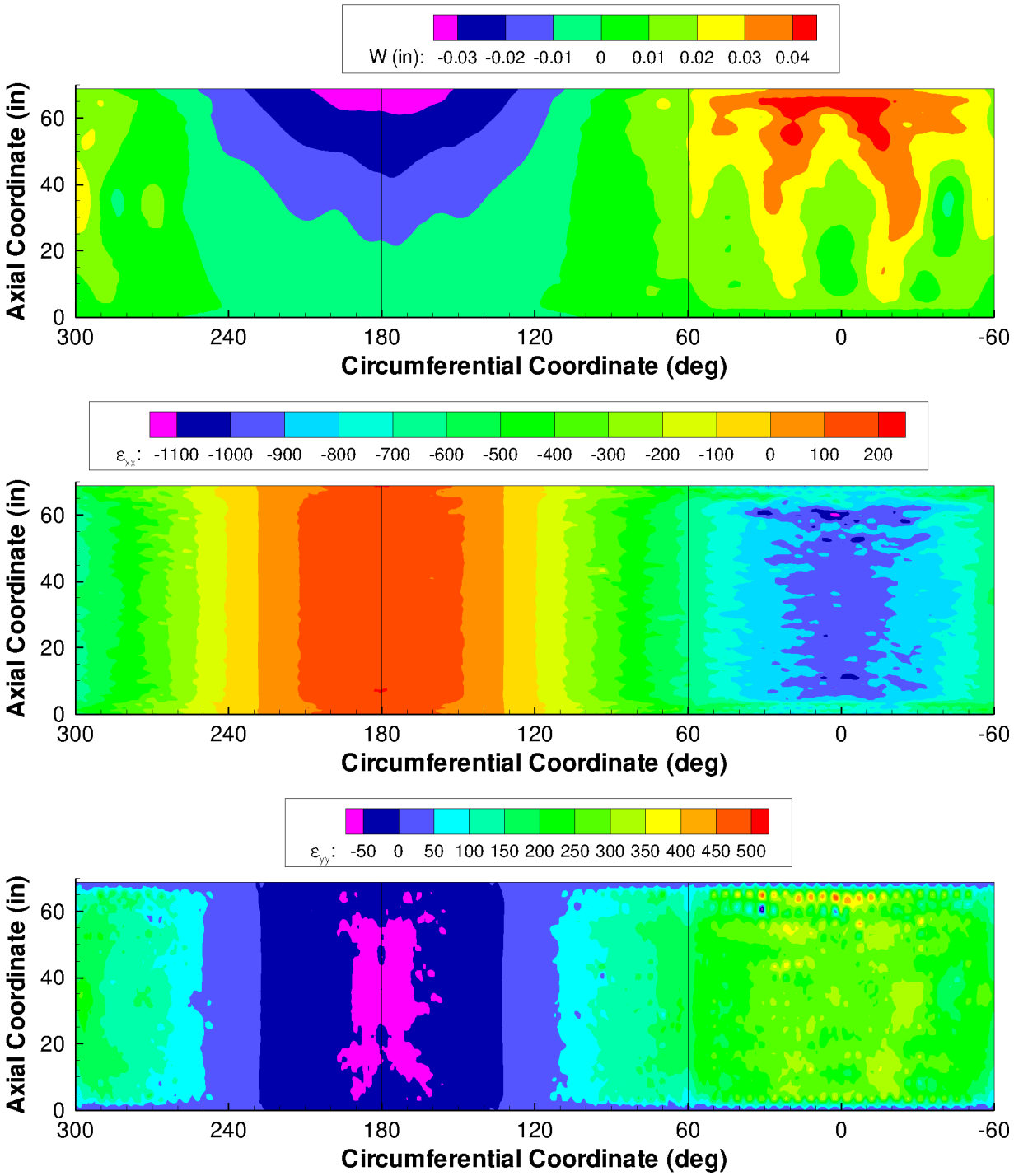

Figure 2.10. Predicted out-of-plane deformation and outer surface strains for the TA under axial loading and positive bending at 0.2 P_{cr} + 0.3 M_{cr}.

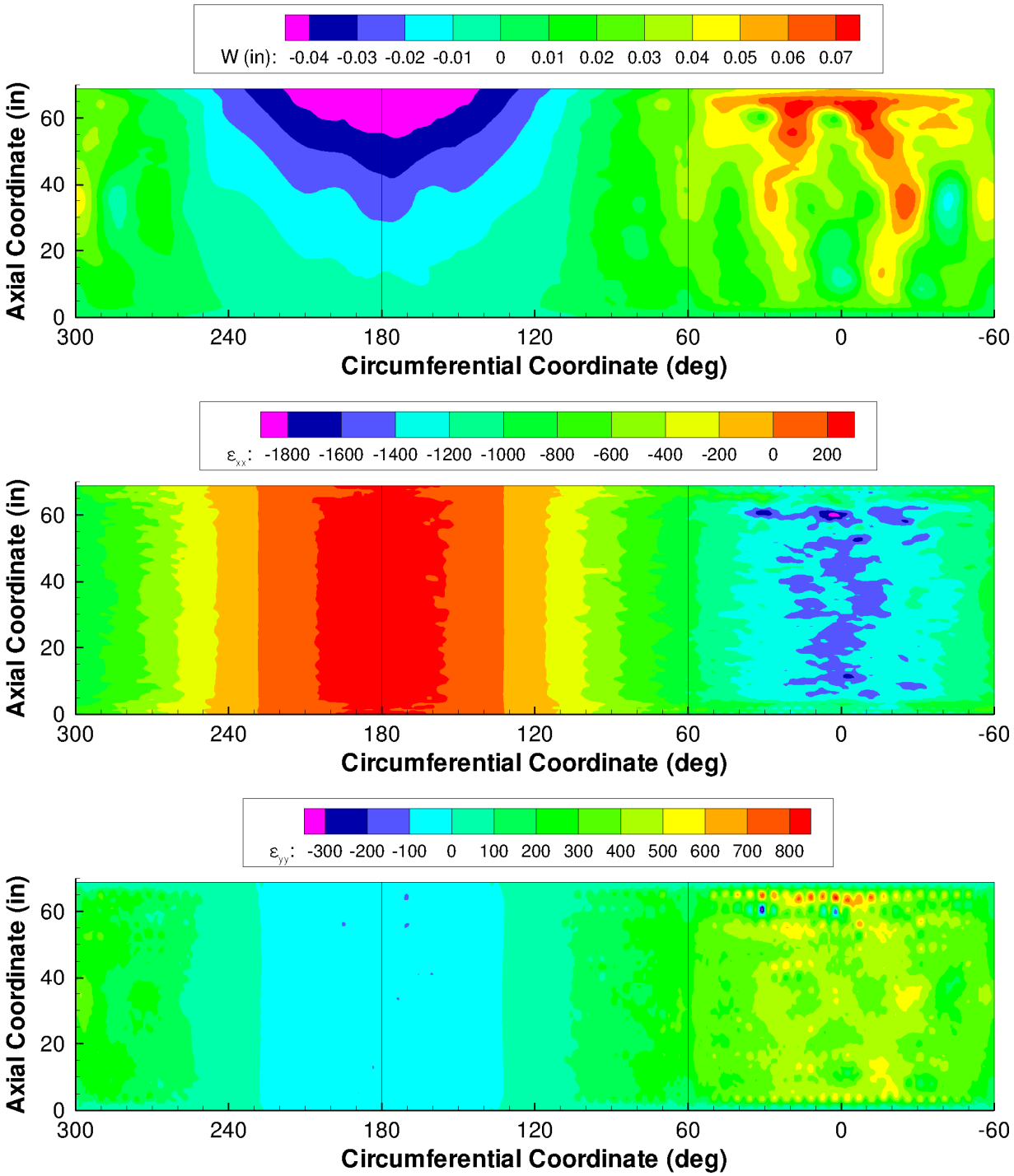

Figure 2.11. Predicted out-of-plane deformation and outer surface strains for the TA under axial loading and positive bending at 0.3 P_{cr} + 0.45 M_{cr}.

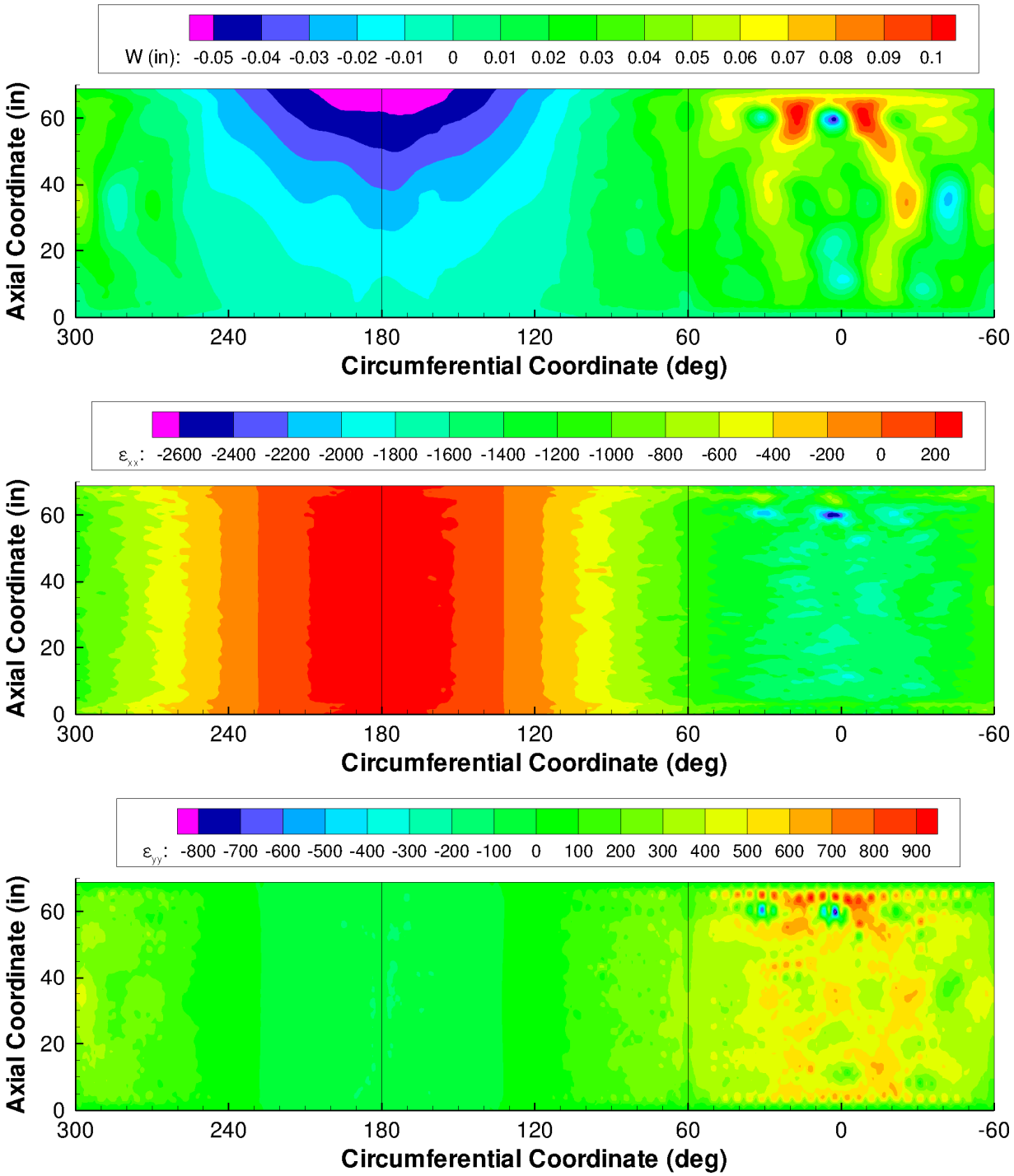

Figure 2.12. Predicted out-of-plane deformation and outer surface strains for the TA under axial loading and positive bending at limit load.

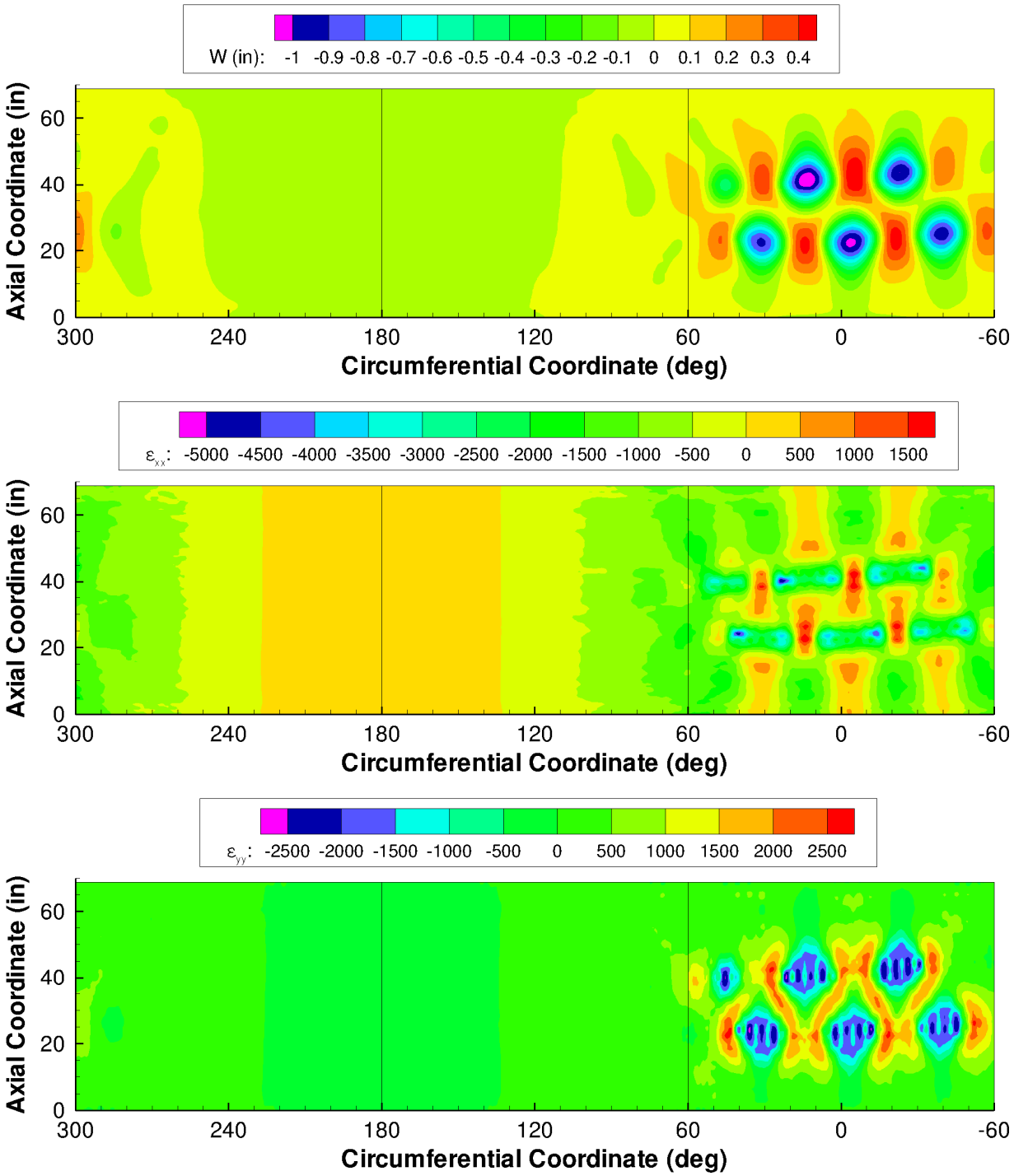

Figure 2.13. Predicted out-of-plane deformation and outer surface strains for the TA under axial loading and positive bending after buckling.

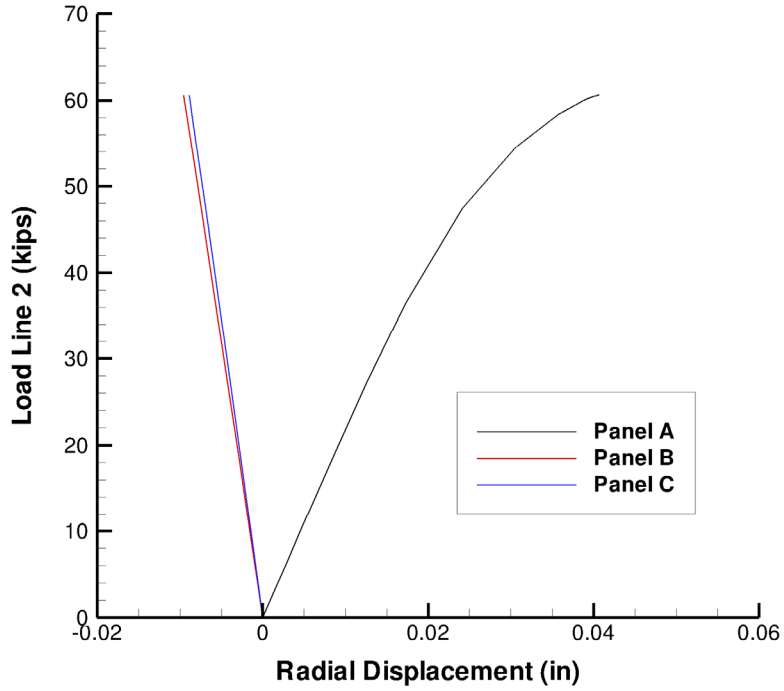

Figure 2.14. Predicted out-of-plane displacement at the center of the panels during combined axial loading and positive bending.

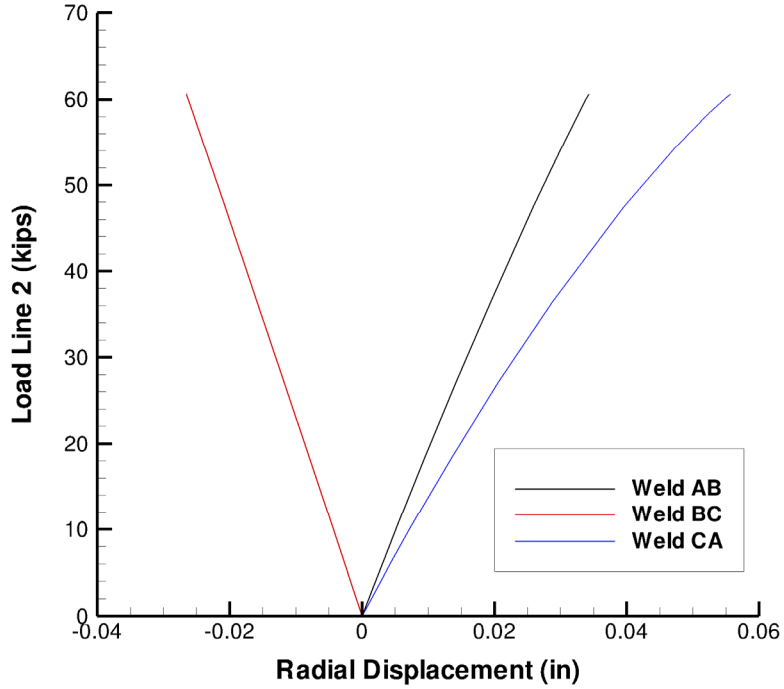

Figure 2.15. Predicted out-of-plane displacement at the center of the axial weld lands during combined axial loading and positive bending.

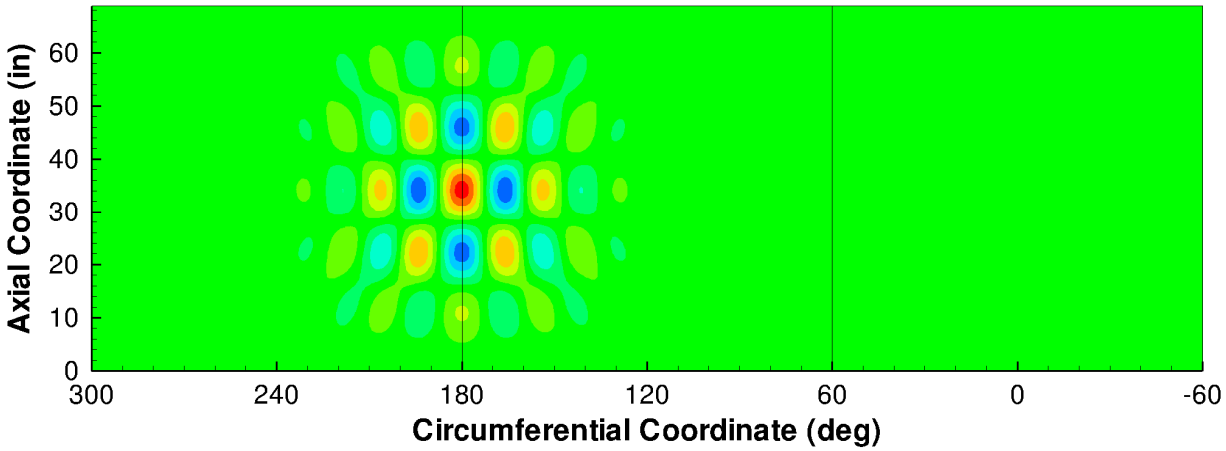

Figure 2.16. Predicted buckling mode shape for the TA under combined axial loading and negative bending.

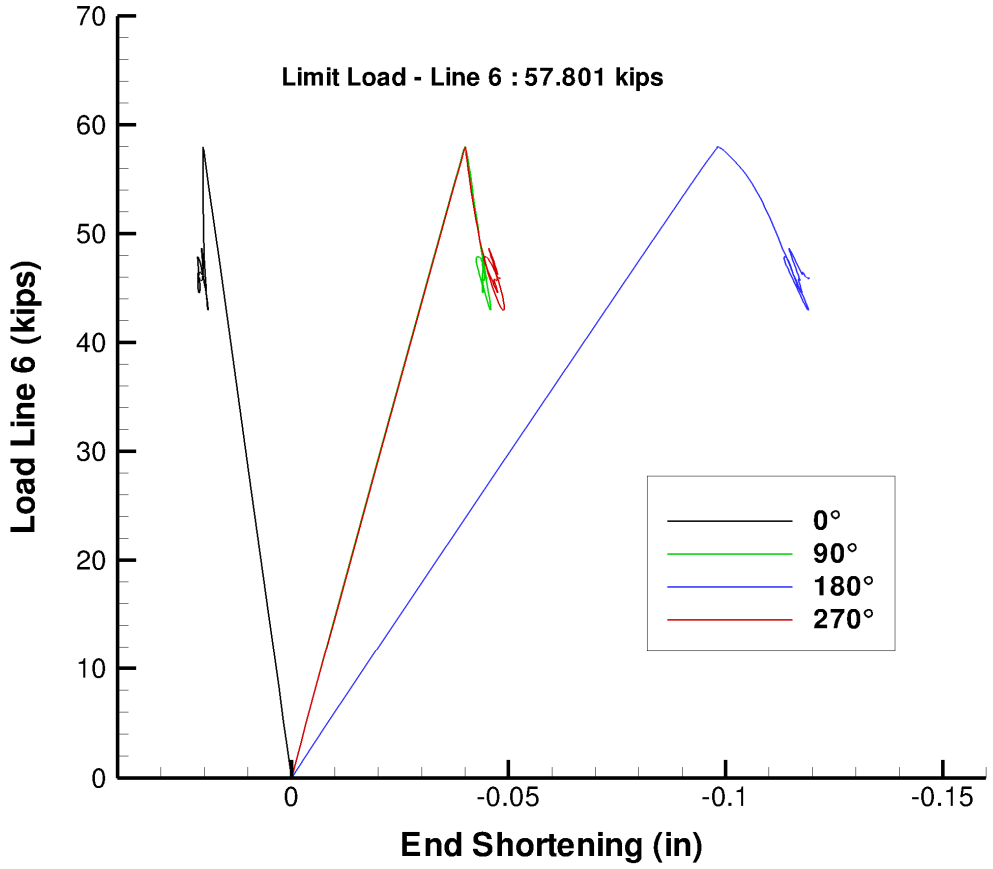

Figure 2.17. Predicted load-shortening response for the TA under combined axial loading and negative bending.

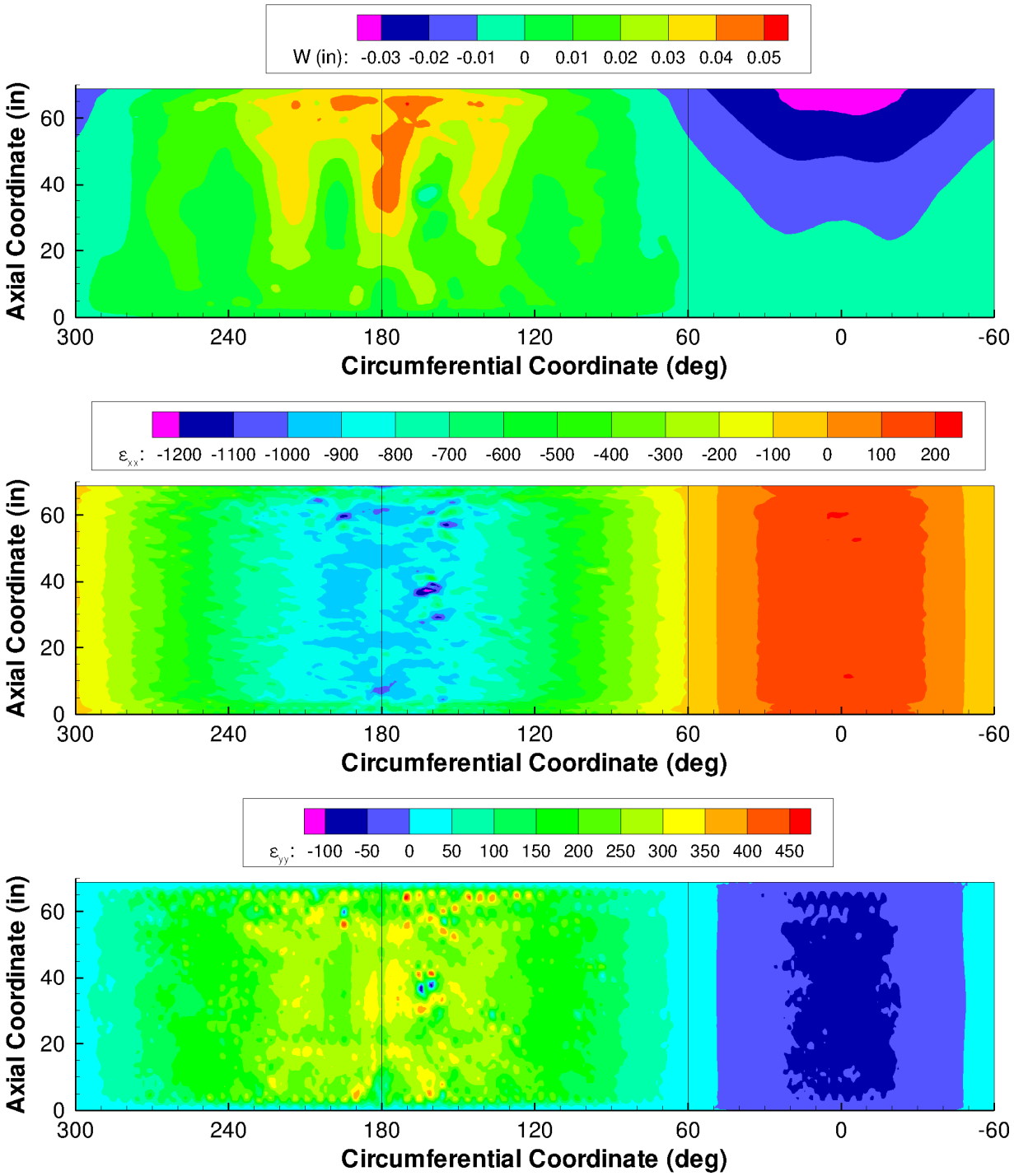

Figure 2.18. Predicted out-of-plane deformation and outer surface strains for the TA under axial loading and negative bending at 0.2 P_{cr} – 0.3 M_{cr}.

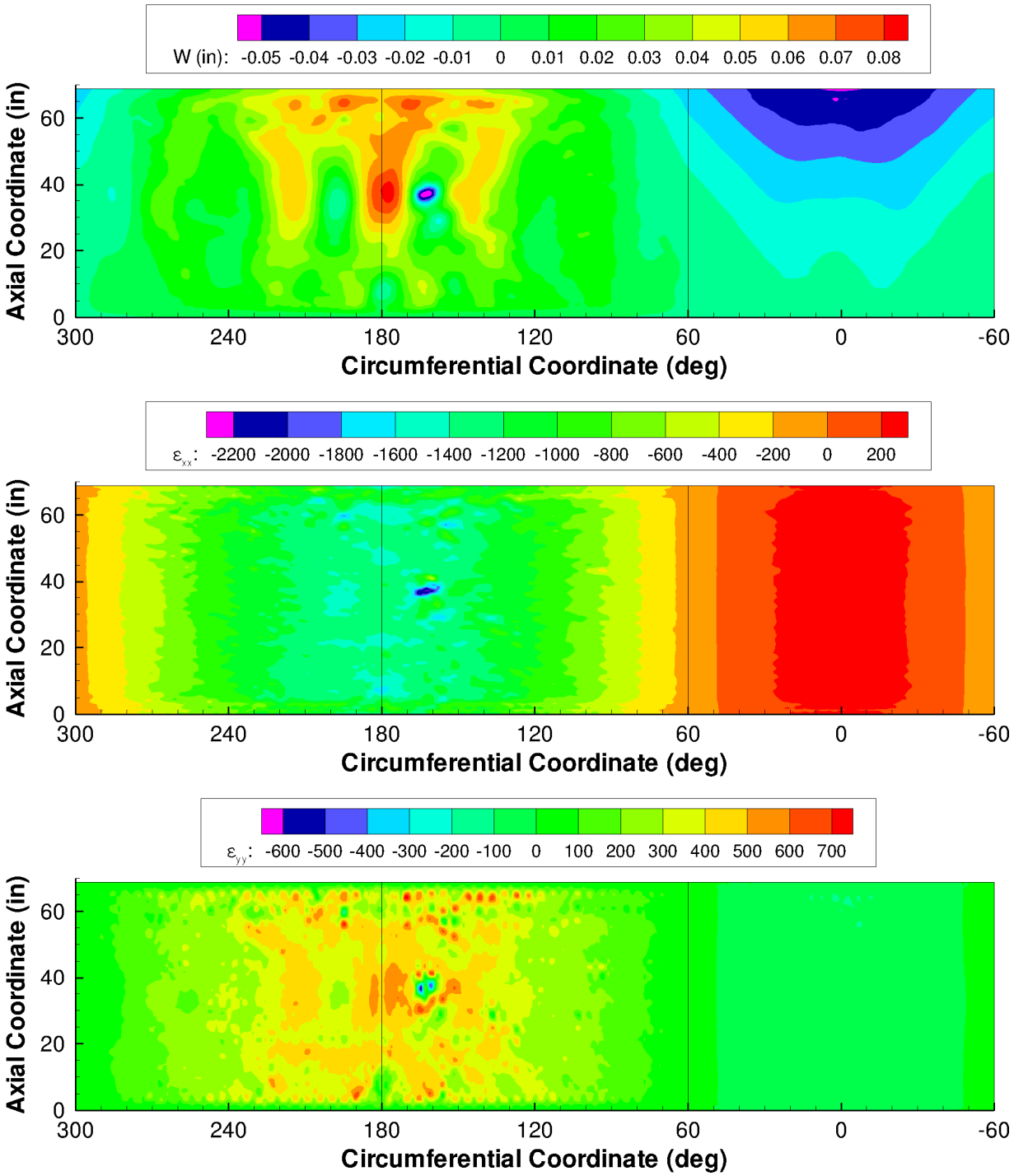

Figure 2.19. Predicted out-of-plane deformation and outer surface strains for the TA under axial loading and negative bending at 0.3 P_{cr} – 0.45 M_{cr}.

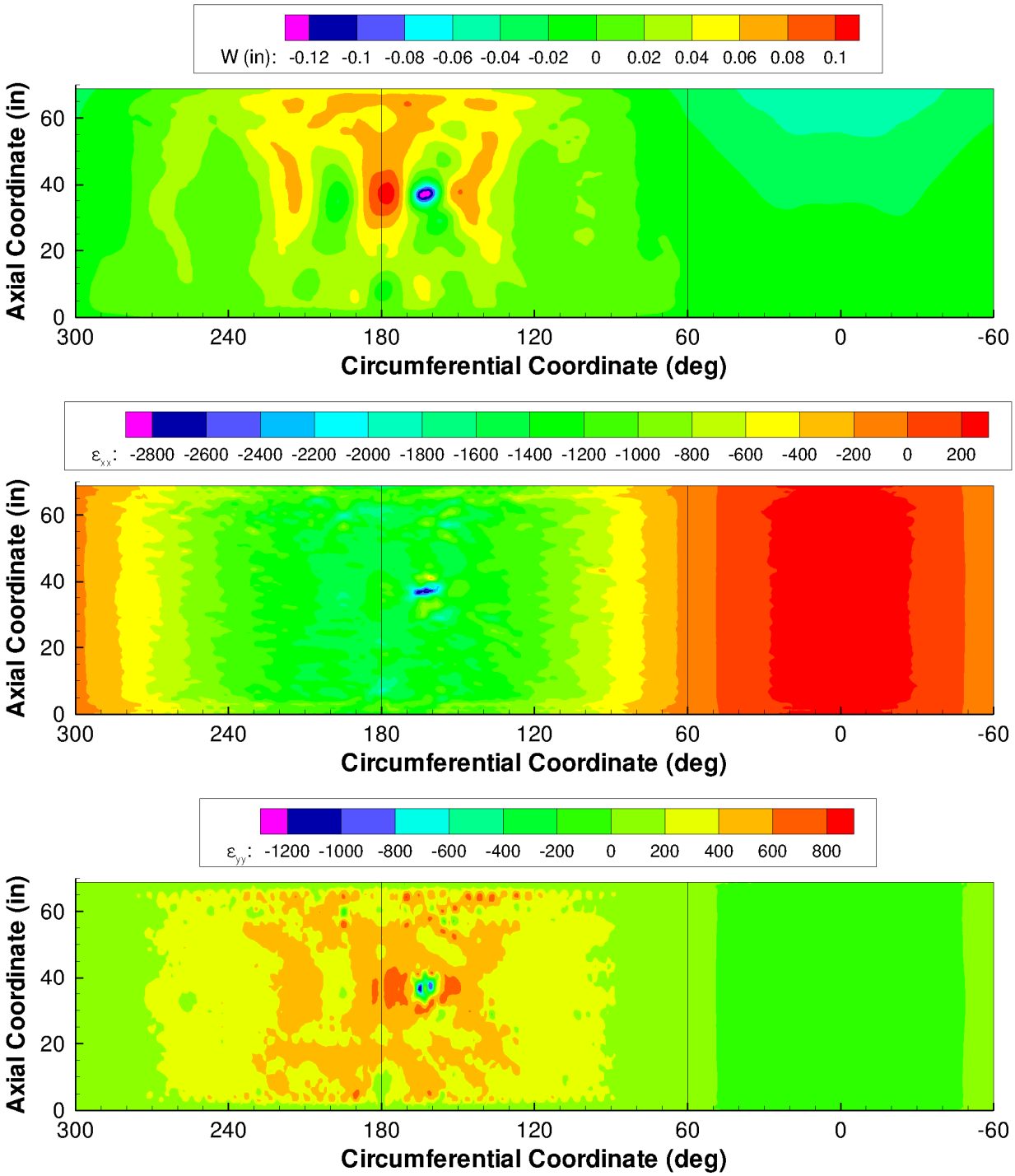

Figure 2.20. Predicted out-of-plane deformation and outer surface strains for the TA under axial loading and negative bending at limit load.

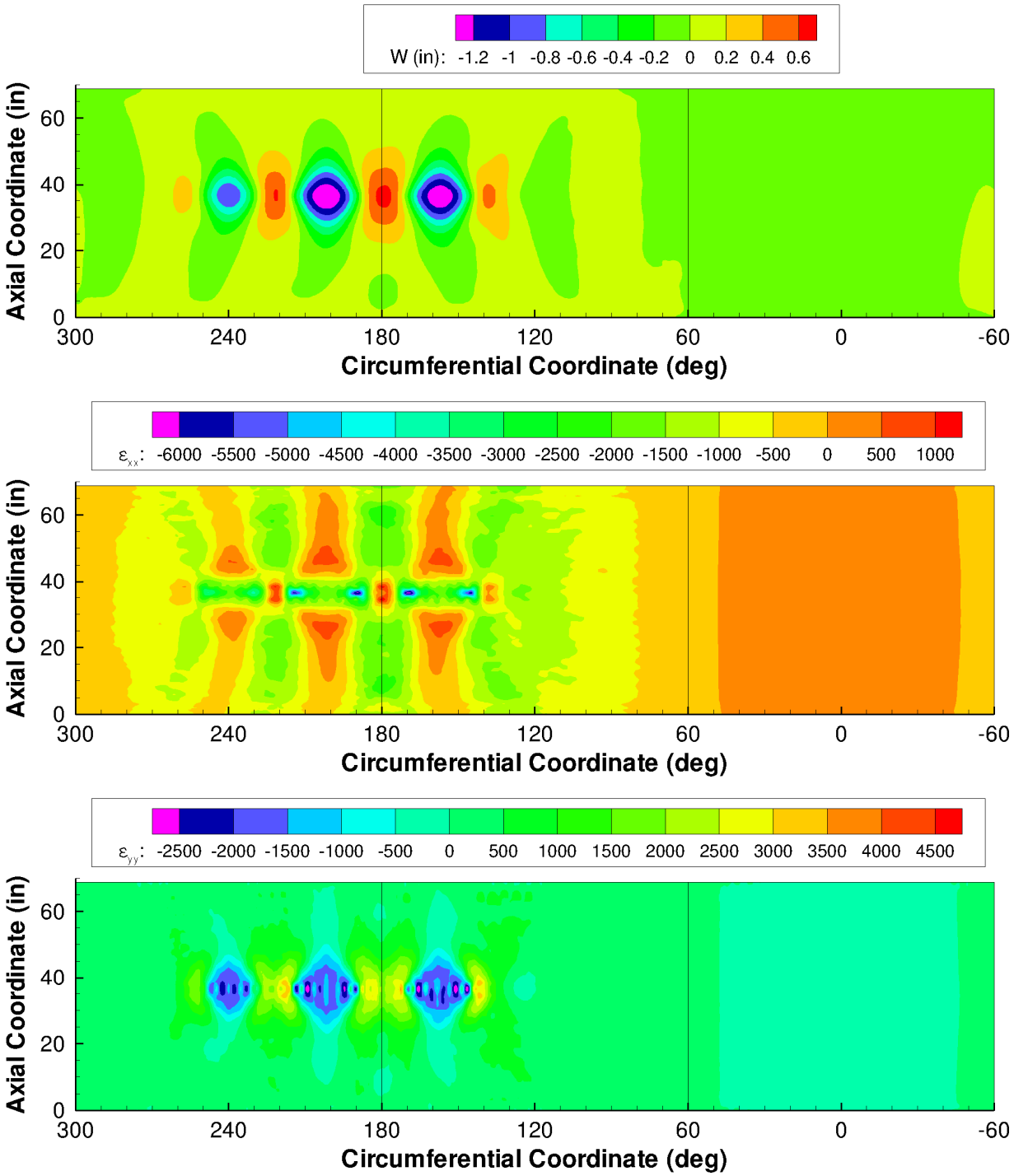

Figure 2.21. Predicted out-of-plane deformation and outer surface strains for the TA under axial loading and negative bending after buckling.

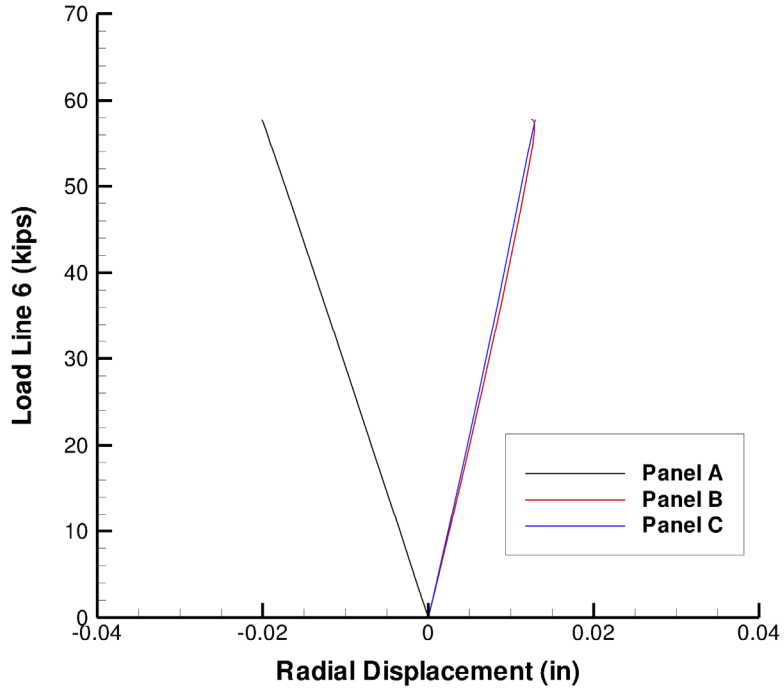

Figure 2.22. Predicted out-of-plane displacement at the center of the panels during combined axial loading and negative bending.

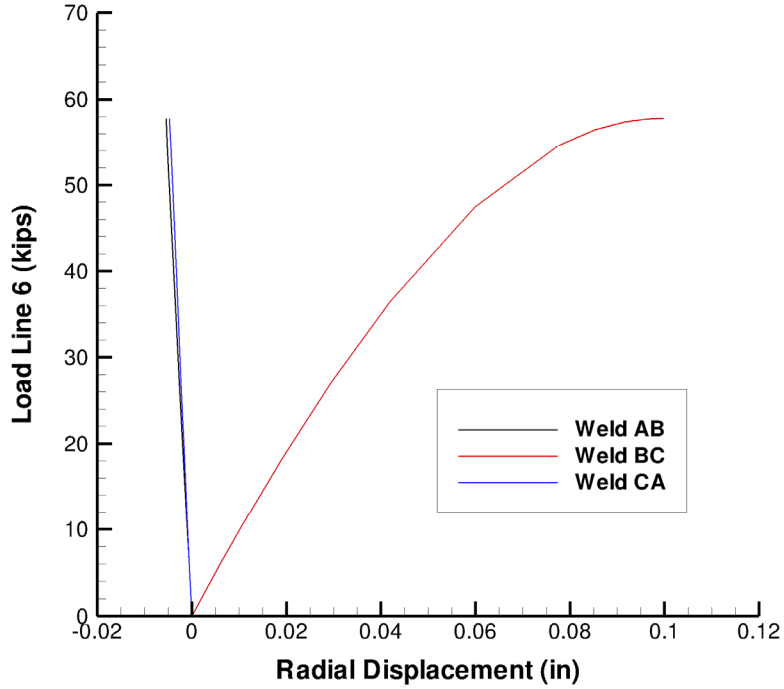

Figure 2.23. Predicted out-of-plane displacement at the center of the axial weld lands during combined axial loading and negative bending.

3.0 References

1. Thornburgh, R. P.; and Hilburger, M. W.: *Design of Orthogrid Cylinder Test Articles for the Shell Buckling Knockdown Factor Assessment*. NASA/TM-2010-216866, November 2010.

REPORT DOCUMENTATION PAGE

Form Approved
OMB No. 0704-0188

1. REPORT DATE *(DD-MM-YYYY)*	2. REPORT TYPE	3. DATES COVERED *(From - To)*
01- 01 - 2011	Technical Memorandum	

4. TITLE AND SUBTITLE

Pre-Test Analysis Predictions for the Shell Buckling Knockdown Factor Checkout Tests - TA01 and TA02

5a. CONTRACT NUMBER

5b. GRANT NUMBER

5c. PROGRAM ELEMENT NUMBER

6. AUTHOR(S)

Thornburgh, Robert P.; Hilburger, Mark W.

5d. PROJECT NUMBER

5e. TASK NUMBER

5f. WORK UNIT NUMBER

869021.04.07.01.13

7. PERFORMING ORGANIZATION NAME(S) AND ADDRESS(ES)

NASA Langley Research Center
Hampton, VA 23681-2199

U.S. Army Research Laboratory
Vehicle Technology Directorate
NASA Langley Research Center
Hampton, VA 23681-2199

8. PERFORMING ORGANIZATION REPORT NUMBER

L-19958

9. SPONSORING/MONITORING AGENCY NAME(S) AND ADDRESS(ES)

National Aeronautics and Space Administration
Washington, DC 20546-0001
and U.S. Army Research Laboratory
Adelphi, MD 20783-1145

10. SPONSOR/MONITOR'S ACRONYM(S)

NASA

11. SPONSOR/MONITOR'S REPORT NUMBER(S)

NASA/TM-2011-216875 ARL-TR-5123

12. DISTRIBUTION/AVAILABILITY STATEMENT

Unclassified -Unlimited
Subject Category - 16 Space Transportation and Safety
Availability: NASA CASI (443) 757-5802

13. SUPPLEMENTARY NOTES

14. ABSTRACT

This report summarizes the pre-test analysis predictions for the SBKF-P2-CYL-TA01 and SBKF-P2-CYL-TA02 shell buckling tests conducted at the Marshall Space Flight Center (MSFC) in support of the Shell Buckling Knockdown Factor (SBKF) Project, NASA Engineering and Safety Center (NESC) Assessment. The test article (TA) is an 8-foot-diameter aluminum-lithium (Al-Li) orthogrid cylindrical shell with similar design features as that of the proposed Ares-I and Ares-V barrel structures. In support of the testing effort, detailed structural analyses were conducted and the results were used to monitor the behavior of the TA during the testing. A summary of predicted results for each of the five load sequences is presented herein.

15. SUBJECT TERMS

Linear variable differential transformer; Shell Buckling Knockdown Factor; Test article; NASA Engineering and Safety Center

16. SECURITY CLASSIFICATION OF:			17. LIMITATION OF ABSTRACT	18. NUMBER OF PAGES	19a. NAME OF RESPONSIBLE PERSON
a. REPORT	b. ABSTRACT	c. THIS PAGE			STI Help Desk (email: help@sti.nasa.gov)
					19b. TELEPHONE NUMBER *(Include area code)*
U	U	U	UU	47	(443) 757-5802